

Evaluation of Soil Moisture in CMIP6 Simulations

LIANG QIAO,^{a,b} ZHIYAN ZUO,^{a,c} AND DONG XIAO^b

^a Department of Atmospheric and Oceanic Sciences/Institute of Atmospheric Sciences, Fudan University, Shanghai, China

^b State Key Laboratory of Severe Weather, Chinese Academy of Meteorological Sciences, Beijing, China

^c Collaborative Innovation Center on Forecast and Evaluation of Meteorological Disasters, Nanjing University of Information Science and Technology, Nanjing, China

(Manuscript received 29 October 2020, in final form 1 November 2021)

ABSTRACT: This study employs multiple reanalysis datasets to evaluate the global shallow and deep soil moisture in Coupled Model Intercomparison Project phase 6 (CMIP6) simulations. The multimodel ensemble mean produces generally reasonable simulations for overall climatology, wet and dry centers, and annual peaks in the melt season at mid- to high latitudes and the rainy season at low latitudes. The simulation capability for shallow soil moisture depends on the relationship between soil moisture and the difference between precipitation and evaporation ($P - E$). Although most models produce effective simulations in regions where soil moisture is significantly related to the $P - E$ (e.g., Europe, low-latitude Asia, and the Southern Hemisphere), considerable discrepancies between simulated conditions and reanalysis data occur at high elevations and latitudes (e.g., Siberia and the Tibetan Plateau), where cold-season processes play a driving role in soil moisture variability. These discrepancies reflect the lack of information concerning the thaw of snow and frozen ground in the reanalyzed data and the inability of models to simulate these processes. The models also perform poorly in areas of extreme aridity. On a global scale, the majority of models provide consistent and capable simulations owing to the minimal variability in deep soil moisture and limited observational information in reanalysis data. Models with higher spatial resolution do not exhibit closer agreement with the reanalysis data, indicating that spatial resolution is not the first limiting factor for CMIP6 soil moisture simulations.

KEYWORDS: Atmosphere–land interaction; Hydrology; Soil moisture

1. Introduction

As a fundamental variable in land–atmosphere interactions, soil moisture plays a key role in the flux of sensible, latent, and radiant heat, momentum exchange, surface albedo, soil heat capacity, vegetation growth, and transpiration, all of which serve to influence Earth’s climate system (Delworth and Manabe 1988; Mahfouf 1991; Zuo and Zhang 2007; Zhang et al. 2016). Soil moisture exerts a “memory” effect on the climate system (Koster and Suarez 2001; Orth and Seneviratne 2012), with soil moisture anomalies persisting for weeks or months and potentially revealing patterns of short-term climate behavior (Yeh et al. 1984; Wu et al. 2002; Wu and Dickinson 2004; Zuo and Zhang 2016; Orth and Seneviratne 2014). On a local scale, soil moisture affects atmospheric stability and water vapor content via evaporation, and thereby has a direct influence on precipitation (Brubaker et al. 1993; Eltahir and Bras 1996; Bosilovich and Chern 2006; Findell and Eltahir 2003; Santanello et al. 2009). On a larger scale, soil moisture affects atmospheric circulation by altering the surface energy balance, which further affects patterns of non-local precipitation (Zhang and Zuo 2011). For instance, Douville et al. (2001) and Douville (2002) confirmed the importance of soil moisture in South Asian and African monsoonal precipitation, and Zuo and Zhang (2016) reported on the impact of springtime soil moisture on the East Asian summer monsoon (Liu et al. 2017; Zhou et al. 2020). Soil moisture also plays a key role in extreme high temperature and heat

wave events (Fischer et al. 2007; Hirschi et al. 2011; Ford and Quiring 2014; Berg et al. 2017), wherein dry soil conditions during summer are aggravated by high temperature extremes via the evaporative feedback mechanism (Hauser et al. 2016). Similarly, Zhang et al. (2019) reported a significant correlation between springtime soil moisture conditions in central–eastern China and elevated summertime temperatures over northeastern China.

Due to the importance of soil moisture in climate dynamics, numerous studies have employed numerical models to investigate soil moisture–climate linkages in greater detail. In their comparison of various coupled land–atmosphere numerical experiments, Seneviratne et al. (2006) observed that the “memory” of soil moisture is controlled primarily by the water-holding capacity of soil, and is most prominent in areas with medium soil moisture (relative to extremely arid or humid regions). Hagemann and Stacke (2015) adjusted the soil hydrological program of the ECHAM6/JSBACH global climate model and reported that soil hydrological processes are more faithfully simulated when soil depth is increased. For example, in humid areas characterized by dense vegetation, deeper soil layers might provide a stronger buffer for soil moisture, thereby improving soil moisture memory. Conversely, greater depth might serve to enhance evaporation from bare soils in sparsely vegetated environments, thereby reducing the soil moisture memory. Using the CMIP5 generation of models, Nakaegawa (2017) made a statistical assessment of future soil moisture conditions in East Asia, the results of which project a significant increase for inland areas of northwestern China and a strong decrease in South and North China. More recently, Zhao et al. (2019) demonstrated how

Corresponding author: Zhiyan Zuo, zuozhy@fudan.edu.cn

DOI: 10.1175/JCLI-D-20-0827.1

© 2021 American Meteorological Society. For information regarding reuse of this content and general copyright information, consult the AMS Copyright Policy (www.ametsoc.org/PUBSReuseLicenses).

the ability of the ACCESS-S1 climate model to forecast maximum and minimum surface temperature, evapotranspiration, and precipitation is improved by incorporation of JULES off-line soil moisture data. Furthermore, [Seo et al. \(2019\)](#) showed that incorporation of true soil moisture conditions into the GloSea5 forecasting system can refine forecasts of summer temperature in both North America and Eurasia.

The Coupled Model Intercomparison Project phase 6 (CMIP6) is an initiative of the World Climate Research Programme Coupling Simulation Working Group. With the goal of “promoting model development and enhancing scientific understanding of the global climate system,” CMIP6 oversees the standardized testing of climate models, formulation of shared data formats, and sharing of climate simulation data within the global scientific community ([Eyring et al. 2016](#); [Zhou et al. 2019](#)). Recognizing that CMIP is a powerful resource for investigating the climate system and projecting future climate change ([Taylor et al. 2012](#)), the models nonetheless contain numerous systematic biases and uncertainties ([van den Hurk et al. 2016](#)). This is particularly true for terrestrial hydrology ([Mueller and Seneviratne 2014](#)). For example, due to model parameterization, multiple hydrological processes have been omitted from simulations, including lateral groundwater flow, lateral flow of reinfiltrating river water, and irrigation with river water, resulting in greater uncertainties in modeled soil moisture ([Zampieri et al. 2012](#); [Greve et al. 2014](#); [Clark et al. 2015](#)). In addition to systematic bias, CMIP models employ various structures and physical parameterization schemes ([Gleckler et al. 2008](#); [Jamison and Kravtsov 2010](#)), with the result that data output can be highly variable among different models. It is essential, therefore, that CMIP simulations are subjected to rigorous evaluation. [Yuan and Quiring \(2017\)](#) employed a combination of observational and satellite data to evaluate soil moisture conditions in CMIP5 simulations for the United States, and reported that, although the models can reproduce seasonal variability in soil moisture, the simulations exhibit significant regional differences.

To date, a comprehensive evaluation of global soil moisture in CMIP6 simulations has yet to be conducted. To address this shortcoming and facilitate the use of these frontline models in future simulations, this study employed reanalysis data to assess CMIP6 soil moisture output. All datasets, CMIP6 models, and methods are described in [section 2](#); results of the evaluation are presented in [section 3](#); the discussion and summary are provided in [section 4](#).

2. Data and methods

a. Data

To evaluate the performance of CMIP6 simulations in modeling soil moisture, this study utilized historical experiment output data for moisture in the upper portion of the soil column (mrsos) and total water content of the soil layer (mrsol). Within the CMIP6 framework, mrsos is defined as the soil moisture to a depth of 10 cm, whereas mrsol has

variable layer number and thickness depending on the specific model. To facilitate the evaluation, the soil moisture is subdivided into shallow and deep soil moisture. In total, 26 models with shallow soil moisture and 25 models with deep soil moisture are employed, which incorporate 192 and 244 members, respectively. Details of each CMIP6 model, member numbers, land models, and spatial resolutions are given in [Table 1](#). The evaluation is based on monthly data collected between 1979 and 2014.

Because soil moisture is hard to measure and highly spatially variable, long-term and large-scale observational data are relatively scarce. The three reanalysis datasets used here—the European Centre for Medium-Range Weather Forecasts (ECMWF) interim reanalysis (ERA-Interim) and most recent reanalysis (ERA5), and the Global Land Data Assimilation System Noah 2.0 (GLDAS-NOAH 2.0)—have been evaluated extensively in previous studies ([Albergel et al. 2012](#); [Liu et al. 2014](#); [Peng et al. 2015](#); [Bi et al. 2016](#); [Cheng et al. 2019](#); [Deng et al. 2020](#); [Fu et al. 2020](#); [Wu et al. 2021](#)). Therefore, the CMIP6 simulated soil moisture is evaluated using these three reanalyses. However, it is noted that soil moisture inevitably has uncertainty and deviation among the reanalyses, which is mainly affected by different assimilation schemes and land surface models in the condition of lack of observations. To minimize this uncertainty, the CMIP6 models will be compared and evaluated against the three different reanalysis datasets. Both ERA-Interim and ERA5 are derived from ECMWF, which incorporates soil moisture data from in situ observations of the global SYNOP network ([Hersbach et al. 2020](#)). As the most recent ECMWF release, ERA5 represents the fifth generation of reanalysis data for global climate and weather. Intended as a replacement for ERA-Interim, ERA5 includes various improvements including new observational data inputs, a greater degree of satellite data integration, and upgrades to the assimilation system and land model (from TESSEL to HTESSEL). ERA5 is the first ECMWF reanalysis including remotely sensed observations, with backscatter (level 1B) from scatterometers providing soil moisture over land in a soil moisture analysis ([Hersbach et al. 2020](#)). The spatial resolution of both ERA5 and ERA-Interim is $0.25^\circ \times 0.25^\circ$; soil moisture is divided into four vertical layers, with sequential ranges of 0–7, 7–28, 28–100, and 100–289 cm.

GLDAS-NOAH 2.0, provided by the National Aeronautics and Space Administration (NASA), is based on satellite and observational data, and employs the advanced offline Noah land surface model to output land surface parameters (e.g., soil moisture). At present, the GLDAS output parameters do not assimilate any observational data, but satellite-based hydrological products (including soil moisture) will be incorporated in the future. The GLDAS soil moisture exhibits a spatial resolution of $0.25^\circ \times 0.25^\circ$ and is divided into four vertical layers, with sequential ranges of 0–10, 10–40, 40–100, and 100–200 cm. Since the thickness of mrsos is defined as 10 cm in CMIP6, the thickness of first layer in GLDAS is also 10 cm, and in ERA5 is 7 cm. To minimize error due to the linear difference and to facilitate calculation, we set shallow soil

TABLE 1. CMIP6 models with, from left to right, their latitude grid points, longitude grid points, land model, and numbers of model variable members employed in this research. (Expansions of many acronyms are available online at <http://www.ametsoc.org/PubsAcronymList>.)

Model	Lat	Lon	Land model	mrsos	mrsol	pr	evspsbl	mrros	snm
ESM-CM2	144	192	CABLE	2	2	3	3	3	3
ESM-ESM1-5	145	192	CABLE	3	3	10	10	29	29
BCC-CSM2-MR	160	320	BCC-AVIM2	3	3	3	3	3	3
BCC-ESM1	64	128	BCC-AVIM2	3	3	3	3	3	3
CAMS-CSM1-0	160	320	CoLM	1		3	3	2	
CanESM5	64	128	CLASS	25	25	25	25	23	65
CAS-ESM2-0	128	256	CoLM	4		4	4		
CESM2	192	288	CLM5	11	11	11	11	11	9
CESM2-FV2	96	144	CLM5		3	3	3	3	1
CESM2-WACCM	192	288	CLM5	3	3	3	3	3	3
CESM2-WACCM-FV2	96	144	CLM5		3	3	3	3	1
CNRM-CM6-1	128	256	ISBA	30	28	30	30		
M-CM6-1-HR	360	720	ISBA	1	1	1	1		
ESM-ESM2-1	128	256	ISBA		10	11	10		
E3SM-1-0	180	360	CLM4.5	5		5	5	5	
E3SM-1-1-ECA	180	360	CLM4.5	1		1	1	1	
FIO-ESM-2-0	192	288	CLM4.9	3		3		3	
GFDL-CM4	180	288	LM4.0	1			1		
GFDL-ESM4	180	288	LM4.1-PPA		1		1		
GISS-E2-1-G	90	144	GISS LSM	12	19	12	12	45	45
GISS-E2-1-G-CC	90	144	GISS LSM	1	1				
GISS-E2-1-H	90	144	GISS LSM	10	10	10	10	25	25
GEM3-GC31-L1	144	192	JULES		4	4	4	4	4
CM6A-LR	143	144	ORCHIDEE LSM	32	32	32	32		
MOC6	128	256	MATSIRO	10	50	50	50	50	50
MPI-ESM-1-2-HAM	96	192	JSBACH	2	2	2	2	3	3
MPI-ESM1-2-HR	192	384	JSBACH	10	10	10	10	10	10
MPI-ESM1-2-LR	96	192	JSBACH	10	10	10	10	10	10
MRI-ESM2-0	160	320	AGCM	5	6	5	5	6	
NorESM2-LM	96	144	CLM5	3	3	3	3	3	
NorESM2-MM	192	288	CLM5	1	1	1	1	3	
CMIP6-MMEM	160	320		192	244	261	259	251	264

moisture to 10 cm. In both the CMIP6 models and reanalysis datasets, the depth of soil moisture can exceed 200 cm. Since increased soil depth potentially reflects soil hydrological processes more truly (Hagemann and Stacke 2015), the deep soil moisture is set to 200 cm. The reanalysis datasets are often less restricted by observations and remote sensing data for deep soil moisture than shallow soil moisture, meaning that the deep soil moisture will be more greatly influenced by the choice of land surface model. To obtain a uniform thickness of soil moisture among the different CMIP6 models and reanalysis datasets, soil moisture within a specific layer is assumed to be evenly distributed, thereby applying a uniform thickness (10 and 200 cm) via the linear difference method (Liu et al. 2014; Zhang et al. 2018), and the unit is uniformly converted to kilograms per square meter.

Meteorological inputs to the evaluation include the variables evaporation (evspsbl), precipitation (pr), surface runoff (mrros), and snowmelt (snm) derived from CMIP6 models, ERA-Interim, ERA5, and GLDAS-NOAH 2.0 (Table 1). Precipitation corresponds to total precipitation, and evaporation is the accumulated amount of water that has evaporated from Earth's surface, including transpiration from vegetation.

b. Methods

To evaluate the CMIP6-derived soil moisture, the globe is divided into 13 regions according to geographical environment and climate (Fig. 1): Siberia (SIB; 50°–75°N, 60°–140°E), inland midlatitude Asia (M-AS; 38°–50°N, 60°–112°E), the Tibetan Plateau (TIB; 30°–38°N, 75°–100°E), low-latitude Asia (L-AS; 10°–30°N, 70°–120°E), North Africa and West Asia (NA-WA; 10°–35°N, 20°W–60°E), Europe (EUR; 35°–70°N, 10°W–60°E), central Africa (C-AF; 15°S–10°N, 20°W–50°E), southern Africa (S-AF; 15°–35°S, 10°–40°E), western North America (WNA; 20°–60°N, 98°–125°W), eastern North America (ENA; 30°–60°N, 60°–98°W), northern South America (NSA; 12°S–10°N, 40°–80°W), southern South America (SSA; 12°–40°S, 40°–65°W), and Australia (AUS; 10°–40°S, 112°–155°E). This assessment does not include Antarctica and Greenland, because data for those regions are missing or incomplete in some CMIP6 models.

Throughout the evaluation, the multimodel ensemble mean (MMEM) is employed to remove uncertainties arising from model differences and initial disturbances. In the process of constructing the CMIP6-MMEM, we considered the weights of different models. The CNRM, for instance, incorporates three

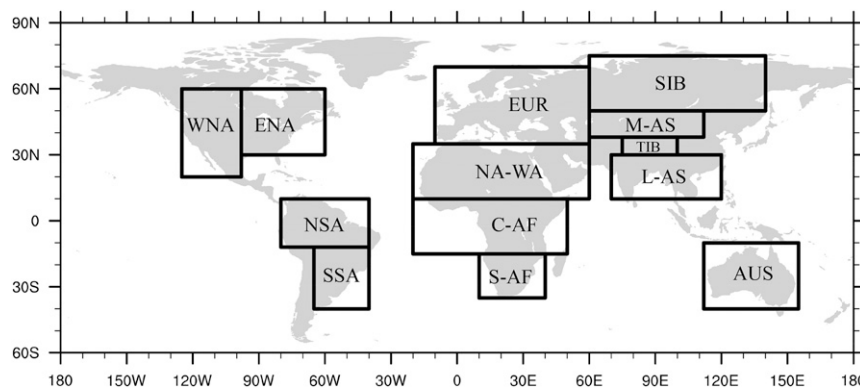


FIG. 1. Major geographical regions defined in this study, the regions are Siberia (SIB: 50°–75°N, 60°–140°E), inland midlatitude Asia (M-AS: 38°–50°N, 60°–112°E), the Tibetan Plateau (TIB: 30°–38°N, 75°–100°E), low-latitude Asia (L-AS: 10°–30°N, 70°–120°E), North Africa and West Asia (NA-WA: 10°–35°N, 20°W–60°E), Europe (EUR: 35°–70°N, 10°W–60°E), central Africa (C-AF: 15°S–10°N, 20°W–50°E), southern Africa (S-AF: 15°–35°S, 10°–40°E), western North America (WNA: 20°–60°N, 98°–125°W), eastern North America (ENA: 30°–60°N, 60°–98°W), northern South America (NSA: 12°S–10°N, 40°–80°W), southern South America (SSA; 12°–40°S, 40°–65°W), and Australia (AUS: 10°–40°S, 112°–155°E).

submodels (CNRM-CM6-1, CNRM-CM6-1-HR, and CNRM-ESM2-1). First, all the submodels of the parent model are averaged, and parent models are further averaged to obtain CMIP6-MMEM. Bias, spatial distribution of the correlation coefficient (COR), Taylor diagrams, and Taylor skill scores (TSS) between CMIP6 simulations and reanalysis data are used primarily for quantitative evaluation. The Taylor diagram (Taylor 2001) intuitively expresses three important statistics [correlation (COR), standard deviation (STD), and root-mean-square error (RMSE)] that are required for graphical model evaluation. To evaluate the simulated temporal variability of soil moisture in different regions from CMIP6 models, the regional-mean time series of CMIP6 models and reanalysis datasets are compared through Taylor diagrams. In this study, the Taylor diagram is standardized. The RMSE and standard deviation of the model in the Taylor diagram are divided by the standard deviation of reanalysis data, respectively. On one hand, the units of standard deviation and RMSE are eliminated. On the other hand, the reference point is changed to 1, so that the values of standard deviation ratio and RMSE in different models are reduced within a certain range, which is more conducive to comparative analysis. The TSS utilizes the COR and STD between the model and reanalysis datasets to evaluate models quantitatively (Taylor 2001), and is calculated as follows:

$$\text{TSS} = \frac{4(1+R)}{\left(\sigma + \frac{1}{\sigma}\right)^2(1+R_0)}, \quad (1)$$

where R is the COR between modeled and reanalysis data, σ is the ratio of modeled STD to the reanalysis data, and R_0 is the theoretical maximum COR, given here as a constant (value = 1). Consequently, TSS values fall between 0 and 1, with higher values reflecting optimal COR and STD, and thus better model simulations.

3. Results

a. Evaluating the spatial distribution of soil moisture climatology

The spatial distribution of the climatology for both shallow and deep soil moisture is evaluated first (Figs. 2 and 3). Figure 2a illustrates the spatial distribution of the annual-mean climate characteristics (1979–2014) for shallow soil moisture (kg m^{-2}) among the different datasets. ERA5, ERA-Interim, GLDAS, and CMIP6-MMEM all exhibit dry centers in typically arid regions, such as NA-WA, S-AF, central AUS, and WNA, in addition to wet centers in typically humid regions, including the high northern latitudes, southeastern China, and NSA. Overall, this alignment confirms that the selected reanalysis data and CMIP6 models can effectively reproduce actual shallow soil moisture conditions. Nonetheless, there are several differences among the different datasets. For example, ERA5 exhibits stronger drought conditions in the dry centers (NA-WA and central AUS) in comparison with the other datasets, whereas the wet centers of ERA-Interim are measurably weaker than in other datasets. Pronounced wet centers are evident in eastern SIB (ERA5), northern SIB (CMIP6-MMEM), and in southeast China (GLDAS).

To further analyze differences in shallow soil moisture between CMIP6-MMEM output and reanalysis data, the ratio of bias [(CMIP6-MMEM – reanalysis data)/CMIP6-MMEM] between CMIP6-MMEM and reanalysis data is analyzed (Fig. 2b). Although this ratio is relatively minor in the Southern Hemisphere and low northern latitudes, indicating a good fit between modeled and reanalysis data, the assessment reveals that a considerable wet bias exists in the middle and high latitudes of the Northern Hemisphere. For example, the ratio of bias between the CMIP6-MMEM and ERA5 is largely negative across South America, the eastern coast of North America, C-

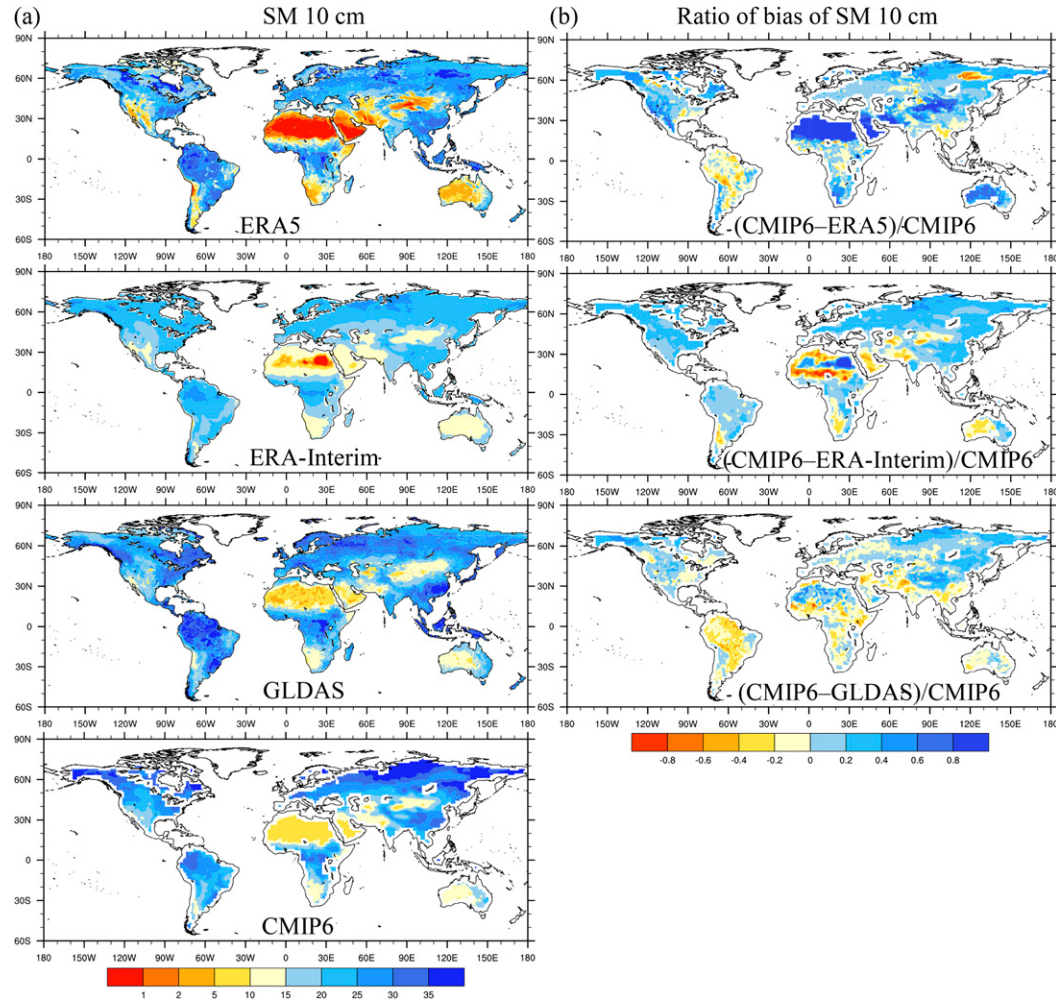


FIG. 2. (a) Spatial distribution of annual-mean climate characteristics (1979–2014) for shallow soil moisture (kg m^{-2}) among the various datasets: (from top to bottom) ERA5, ERA-Interim, GLDAS, and CMIP6-MMEM. (b) Spatial distribution of shallow soil moisture ratio of bias (kg m^{-2}) between CMIP6-MMEM and reanalysis data [$(\text{CMIP6-MMEM} - \text{reanalysis data})/\text{CMIP6-MMEM}$], comparing (from top to bottom) CMIP6-MMEM and ERA5, CMIP6-MMEM and ERA-Interim, and CMIP6-MMEM and GLDAS.

AF, Southeast Asia, in the vicinity of Balkhash Lake, and in eastern SIB, with positive values elsewhere. Similarly, comparison of the CMIP6-MMEM and ERA-Interim reveals a predominantly negative ratio of bias in southern SSA, NA-WA, S-AF, northwest China, and western AUS, but positive values in most other regions. Finally, the bias between the CMIP6-MMEM and GLDAS is largely positive in mid- and high-latitude Eurasia, most of North America, and North Africa, whereas other regions are predominantly negative.

The spatial distribution of annual-mean climate characteristics (1979–2014) for deep soil moisture (kg m^{-2}) among the different datasets is shown in Fig. 3a. Overall, the distribution of dry and wet centers of deep soil moisture is similar to that of shallow soil moisture, suggesting that reanalysis data and CMIP6 models are both capable of reconstructing this parameter. The spatial distribution of the deep soil moisture bias between the

CMIP6-MMEM and reanalysis data is also similar to that of the shallow soil moisture (Fig. 3b).

According to these soil moisture results, clear disparities exist between the CMIP6-MMEM and reanalysis datasets, and among the three different reanalysis datasets. Without considering lateral water exchange between adjacent soil volumes, soil moisture is affected primarily by total precipitation, evapotranspiration, surface runoff, and drainage (Seneyiratne et al. 2010), whereas surface soil moisture is mainly affected by the first three factors. To quantify differences between the CMIP6-MMEM and the reanalysis datasets, three climatological (1979–2014) parameters—precipitation, evaporation, and surface runoff (mm yr^{-1})—in more detail are further analyzed (Fig. 4). Overall, precipitation and evaporation are larger than surface runoff, the latter being close to zero in arid areas. Even in humid areas, surface runoff does not exceed 500 mm yr^{-1} .

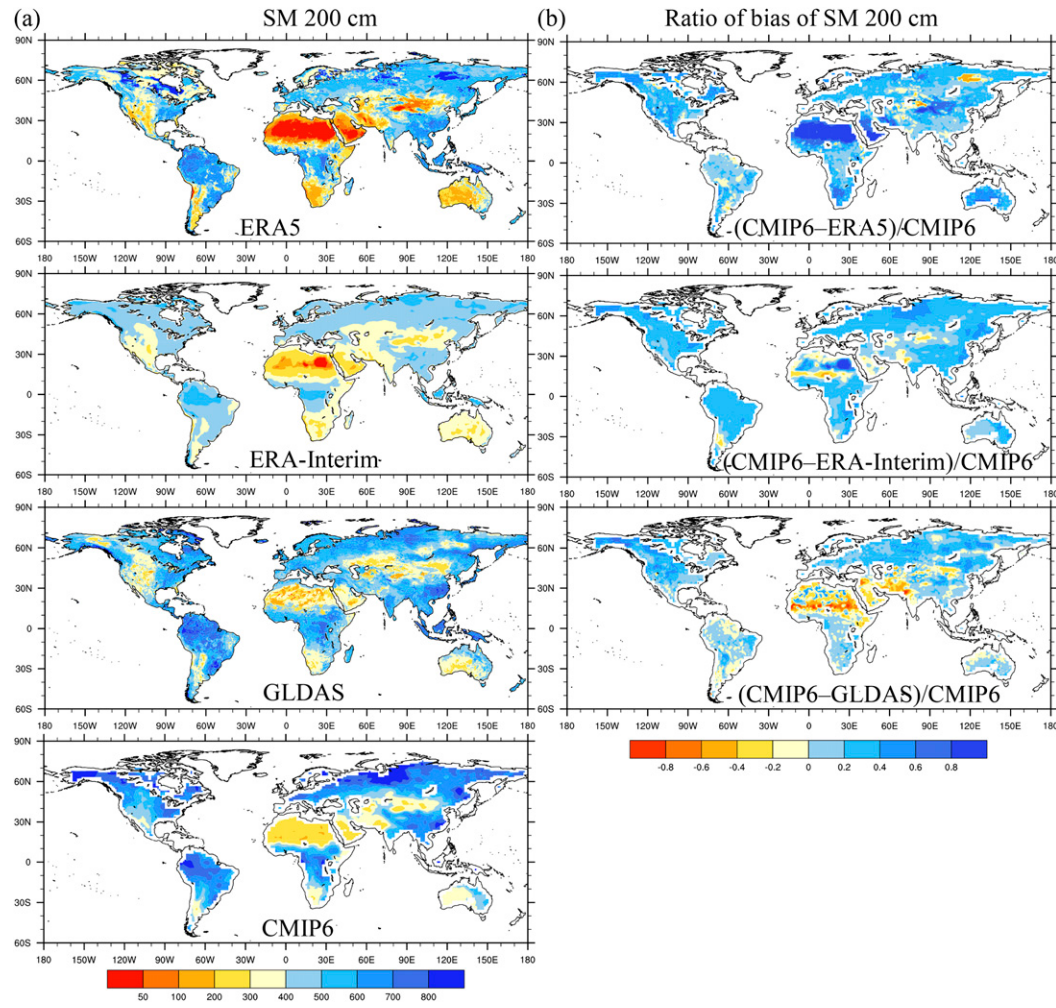


FIG. 3. As in Fig. 2, but for deep soil moisture.

The low- and high-value areas for precipitation, evaporation, and surface runoff generally correspond well to the dry and wet centers of soil moisture, confirming that these three parameters influence soil moisture.

This treatment demonstrates that the bias of elements between CMIP6-MMEM output and reanalysis data can facilitate the interpretation of CMIP6 soil moisture simulations. To do this, first, the bias is calculated by subtracting the CMIP6-MMEM from the reanalyzed data, then the bias is divided by the CMIP6-MMEM [ratio = $(\text{CMIP6} - \text{reanalysis data})/\text{CMIP6}$] to obtain the distribution ratio of bias (Figs. 4b-d). For precipitation, this ratio is primarily positive, with only minor negative biases in South America, C-AF, and the Indian subcontinent, indicating that the CMIP6-MMEM simulation generally exceeds the reanalysis data.

The CMIP6-MMEM for evaporation is relatively variable compared with the three reanalysis datasets. For ERA5, the ratio of bias is largely negative over parts of M-AS and the Indian subcontinent, and positive for parts of N-AF, AUS,

and WNA. The range and value of the ratios are minimal, indicating there is little difference in evaporation between ERA5 and CMIP6-MMEM. In contrast, the large evaporation ratio of bias between the CMIP6-MMEM and ERA-Interim occurs primarily in NA-WA and the Indian subcontinent and is generally negative; positive ratios of bias occur only in a few regions. For the GLDAS, evaporation is dominated by positive ratios, especially in North Africa and M-AS, indicating that the CMIP6-MMEM produces larger evaporation output than GLDAS.

The surface runoff ratio of bias is considerably larger than those of precipitation and evaporation, and, on a global scale, is largely positive. On the one hand, this distribution shows that the CMIP6 models produce higher values of surface runoff than are captured by the reanalysis data. On the other hand, it suggests that the CMIP6 models and reanalysis datasets exhibit greater uncertainty in surface runoff than they do in precipitation and evaporation. Nonetheless, because the magnitude of surface runoff is smaller than both precipitation

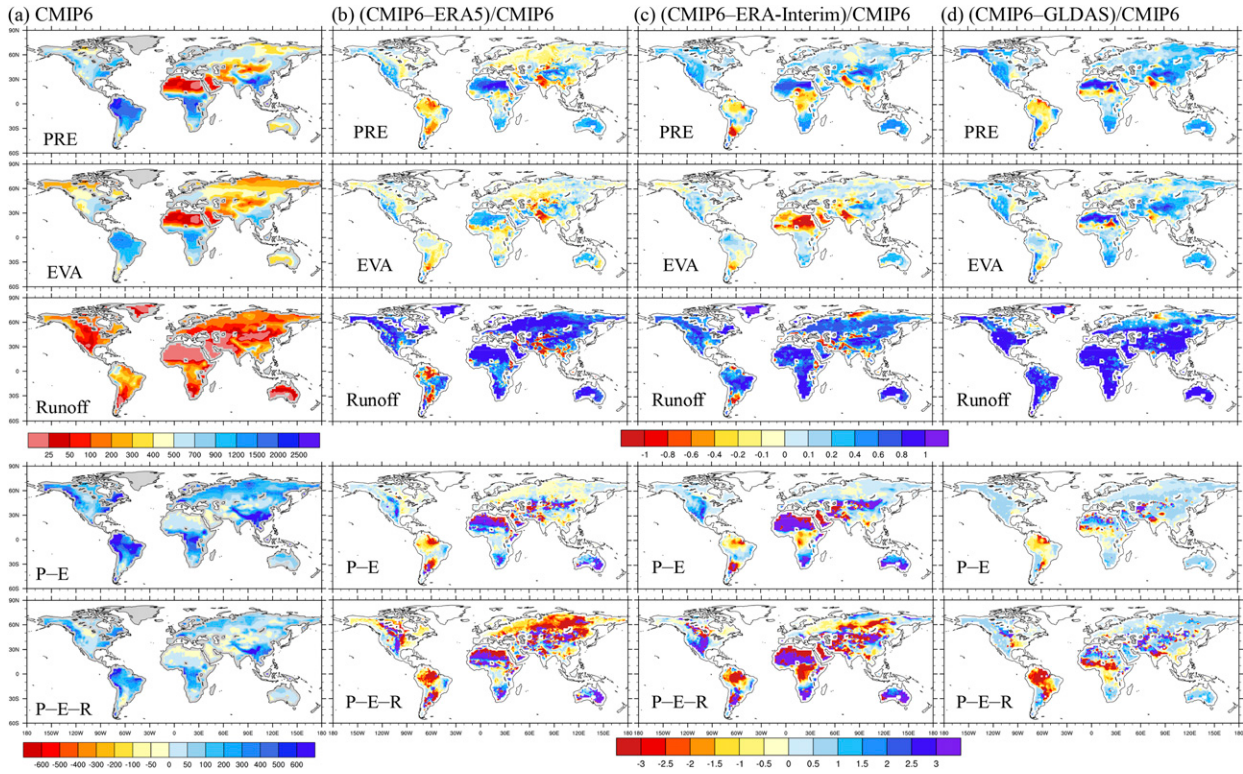


FIG. 4. (a) Spatial distribution (mm yr^{-1}) of annual-mean climate characteristics (1979–2014) for (from top to bottom) precipitation (PRE), evaporation (EVA), surface runoff (runoff), precipitation minus evaporation ($P - E$), and precipitation minus evaporation and surface runoff ($P - E - R$). (b)–(d) Spatial distribution of the ratio of bias between CMIP6-MMEM and reanalysis data [(CMIP6-MMEM – reanalysis data)/CMIP6-MMEM], showing the ratio of bias (b) between CMIP6-MMEM and ERA5, (c) between CMIP6-MMEM and ERA-Interim, and (d) between CMIP6-MMEM and GLDAS. Results are for (from top to bottom) are PRE, EVA, runoff, $P - E$, and $P - E - R$.

and evaporation, the overall influence of surface runoff on soil moisture is limited. Combined with the above analysis, differences in soil moisture between CMIP6-MMEM and reanalysis data can be attributed to precipitation, evaporation, and surface runoff. The CMIP6-MMEM precipitation exceeds the ERA5 and ERA-Interim values, resulting in overall higher soil moisture values in the CMIP6-MMEM. As for the bias of soil moisture between CMIP6-MMEM and GLDAS, the generally low values provided by the former reflect high evaporation.

For this assessment, analyzing the difference between precipitation and evaporation ($P - E$) and the value of precipitation minus evaporation and surface runoff ($P - E - R$) is analyzed from the perspective of surface water balance. For the climatological CMIP6-MMEM (Fig. 4a), the difference between $P - E$ and $P - E - R$ is minimal, especially in arid regions, thereby confirming that surface runoff is negligible relative to $P - E$. The climatological distribution of $P - E$ is similar to that of soil moisture, with high- and low-value centers corresponding to wet and dry centers of soil moisture, indicating that the surface available water plays a key role in soil moisture. Meanwhile, both $P - E$ and $P - E - R$ exhibit weakly negative ratios in generally arid areas, where intense

evaporation causes underground water to move toward the surface, evaporation causes by nonprecipitation such as snowmelt and dew, or where there is a long-term drying trend (Li et al. 2016; Zhang et al. 2015).

For the $P - E$ ratio of bias, high ratios occur primarily in NA-WA and M-AS, as well as parts of AUS, S-AF, and South America, and are generally positive. This ratio corresponds well to the soil moisture bias, indicating that $P - E$ has a significant impact on soil moisture. The $P - E$ ratios for ERA-Interim and ERA5 are larger than for GLDAS, suggesting minimal difference in surface available water between the CMIP6-MMEM and GLDAS. For the $P - E - R$, large ratios occur not only in the areas defined above but also at high latitudes, indicating that the addition of surface runoff increases the uncertainty between the CMIP6-MMEM and reanalysis data, particularly in mid- and high-latitude Eurasia and North America.

Soil moisture values also vary among the different reanalysis datasets. In the absence of observational data, soil moisture values are more dependent on the specific land model and assimilation schemes used, which accounts for the large degree of variance. Although ERA5 and ERA-Interim are both ECMWF products, there are important discrepancies

between them. For example, soil moisture in ERA5 is lower over NA-WA than in ERA-Interim and higher over high latitudes and humid regions. These differences probably reflect the upgraded assimilation scheme and land surface model of ERA5, as well as the improved bare soil evaporation parameter, incorporation of vegetation cover change, and enhanced parameterization of snow cover and runoff (Hersbach et al. 2020). Together, these improvements have enhanced the accuracy of soil moisture in hyper-arid areas with less vegetation coverage, in humid areas with greater runoff, and at high latitudes with deeper snowpack, bringing ERA5 and GLDAS into closer alignment in humid regions and high latitudes. The $P - E$ ratios of ERA5 and ERA-Interim, meanwhile, are higher than that of GLDAS over NA-WA (Figs. 4b–e), meaning that $P - E$ values of the former are smaller than for GLDAS. This result can be attributed to the lower values of surface available water over NA-WA included in the ERA5 and ERA-Interim datasets.

b. Seasonal characteristics of soil moisture

To explore seasonal variability in CMIP6 simulated soil moisture among the different regions, the shallow soil moisture (kg m^{-2}) annual cycle characteristics (1979–2014) of both the CMIP6 models and reanalysis data are analyzed (Fig. 5). Due to the large interregional variability in soil moisture, the vertical axis in Fig. 5 differs according to region. Since ERA-Interim and ERA5 include similar soil moisture characteristics, the analysis detailed below utilizes only the ERA5 dataset. In essence, the CMIP6-MMEM represents the middle point of the various constituent CMIP6 models. Moreover, the CMIP6-MMEM is more closely aligned with reanalysis data than are the individual CMIP6 models, suggesting that this approach effectively filters out uncertainties arising from model differences and initial disturbances.

Overall, the characteristics of seasonal variability in the CMIP6-MMEM are broadly consistent with both ERA5 and GLDAS. A notable exception is the TIB, where there is a significant difference in the timing of peak values (from February to August) among the different models. This phenomenon results in minor seasonal changes in the CMIP6-MMEM, whereas both ERA5 and GLDAS peaked in August. We speculate that this pattern reflects the impact of frozen soil, snow cover, and their melting processes on the TIB in models (see below). The range of shallow soil moisture in ERA5 is less than in both GLDAS and the CMIP6-MMEM, whereas the CMIP6-MMEM values are more similar to GLDAS output.

The different regions covered in this investigation exhibit significant seasonal changes in shallow soil moisture. In mid-to-high northern latitudes (SIB, EUR, WNA, and ENA), the pattern of seasonal variability is broadly similar: shallow soil moisture is highest during winter and spring, with an annual minimum occurring in late summer and early autumn (July–September). In these regions, the high winter–spring moisture content is related to the melting of snow cover and frozen soil, whereas the subsequent low moisture conditions reflect the relatively hot (increasing evaporation), dry conditions

characteristic of late summer and early autumn. These annual characteristics are consistent with the findings of Lu et al. (2005) and Li et al. (2007). At low latitudes (L-AS and NA-WA), the data indicate that this pattern is reversed: shallow soil moisture reaches its annual maximum in July–September and is lowest in spring. The springtime minimum is a direct consequence of low precipitation and increasing evaporation as temperatures rise in spring; the July–September maximum reflects the impact of South and East Asian monsoon precipitation, which in L-AS causes shallow soil moisture in summer to be almost double that in spring. In NA-WA, the late summer–early autumn increase is relatively minor, reflecting the arid prevailing climate of this region.

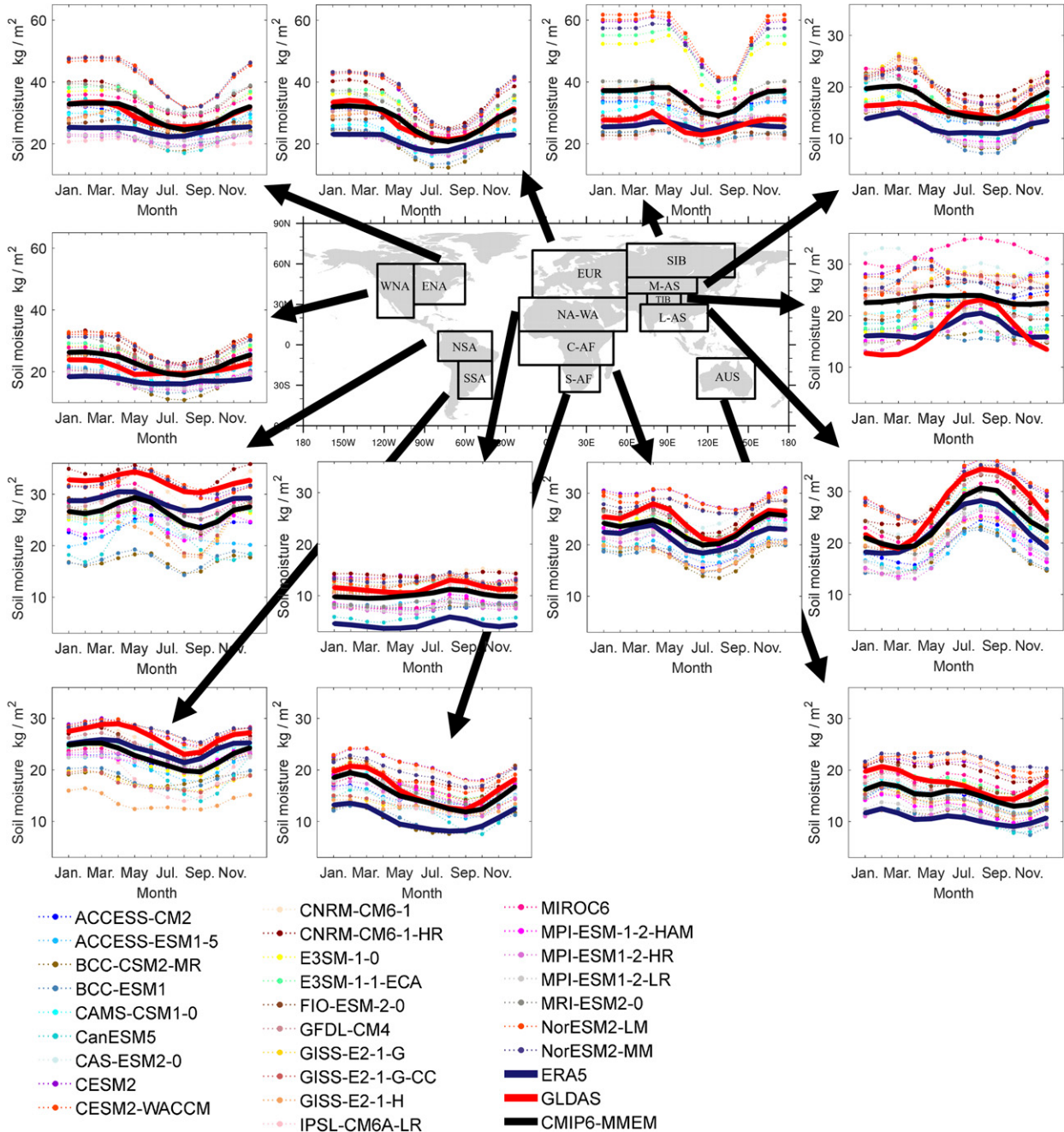
In the Southern Hemisphere, NSA, SSA, C-AF, S-AF, and AUS all exhibit similar seasonal variations in shallow soil moisture. Specifically, annual maximum values occur during April–May in NSA, SSA and C-AF, and in February in S-AF and AUS. Similarly, the annual minimum occurs during July in C-AF and during September–October in NSA, SSA, S-AF, and AUS. The minimum annual cycle of soil moisture in the Southern Hemisphere often occurs in the dry season over Africa, and in the winter and spring over South America and Australia.

Although the range of model-simulated soil moisture varies among different models, they nearly have consistent seasonal characteristics. Meanwhile, Koster et al. (2009) indicate that although the range of soil moisture output from various models forced by the same atmospheric forcing field is diverse, outputs of different models have the same temporal soil moisture variability. It shows that the temporal soil moisture variability of the model output is more important than absolute values, so the subsequent assessment of this study is mainly based on the temporal soil moisture variability. Subsequent analysis of Taylor diagram is conducted through regional-mean time series.

Correspondingly, the annual cycle characteristics (1979–2014) of deep soil moisture (kg m^{-2}) are depicted in Fig. 6. Compared with the majority of CMIP6 models, the range of CMIP6-MMEM output aligns relatively well with the reanalysis data, indicating that the MMEM can also effectively reproduce deep soil moisture. Deep soil moisture does not exhibit significant seasonal variability for most regions, the sole exception being L-AS, where an annual maximum occurs in August–September and a minimum during March–April.

c. Evaluation of regional soil moisture

To further evaluate soil moisture in CMIP6 simulations, Taylor diagram analysis of the CMIP6 models against both the ERA5 and GLDAS datasets is conducted for temporal variability over different regions. Theoretically, greater spatial resolution can enhance the impact of local topography, improve surface heterogeneity, and improve land–atmosphere interactions, improvements that together will strengthen the simulation of soil moisture. Therefore, models are grouped according to their spatial resolution (Table 2) to quantify the impact of this parameter on simulated soil moisture. The Taylor diagram for shallow soil moisture is depicted in Fig. 7. The



disparity between CMIP6-simulated output and both ERA5 and GLDAS reanalysis data is minor in the Southern Hemisphere but large in the Northern Hemisphere. For example, typical Northern Hemisphere COR values fall between -0.60 and 0.30 , and STD and RMSE values range from 1.0 to 4.0 . In contrast, Southern Hemisphere COR values generally fall between 0.60 and 0.95 , and STD and RMSE values range from 0.5 to 1.5 . For the entire CMIP6 array, only three models

(FIO-ESM-2-0, IPSL-CM6A-LR, and MPI-ESM-1-2-HAM) align with ERA5 in the Northern Hemisphere; only the MPI-ESM1-2-HR model aligns with GLDAS. This poor performance among models is mainly derived from the relatively low COR values. In contrast, the offset between modeled and reanalysis data is significantly smaller for the Southern Hemisphere, where not only the COR values are improved (generally >0.60), but the STD and RMSE values are also relatively

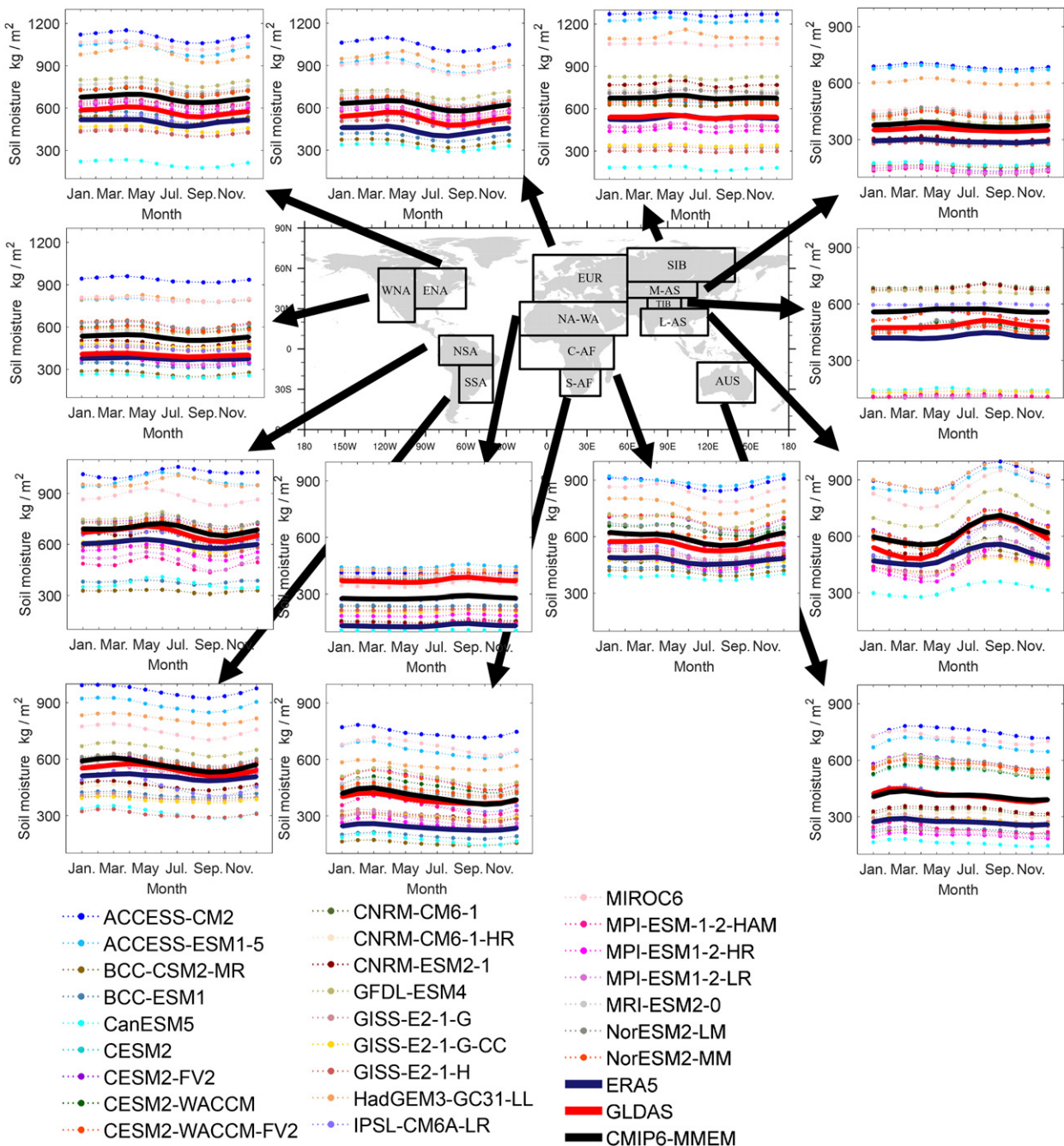


FIG. 6. As in Fig. 5, but for deep soil moisture.

low (generally <1.5) compared with the Northern Hemisphere.

Overall, CMIP6 models are better aligned with GLDAS than with ERA5. For the Northern Hemisphere, COR values for ERA5 and GLDAS reanalysis fall between -0.60 and -0.30 and between -0.30 and 0.60 , respectively. There is no apparent difference in STD and RMSE between the datasets. In contrast, COR values for ERA5 and GLDAS reanalysis in the Southern Hemisphere fall within the ranges 0.60 – 0.85 and

0.75 – 0.95 , respectively. Southern STD and RMSE values are typically between 0.5 and 1.5 for ERA5 and between 0.5 and 1.0 for GLDAS.

Comparison of high and low spatially resolved output reveals no significant difference between the two. The respective COR values are indistinguishable; even the high spatial resolution group returns STD and RMSE values that are slightly larger than those of the low spatial resolution group. Similarly, there are three models incorporating both high and

TABLE 2. CMIP6 model groupings, showing (left) the high-resolution group and (right) the low-resolution group.

High-resolution models	Lat	Lon	Low-resolution models	Lat	Lon
BCC-CSM2-MR	160	320	ACCESS-CM2	144	192
CAMS-CSM1-0	160	320	ACCESS-ESM1-5	145	192
CESM2	192	288	BCC-ESM1	64	128
CESM2-WACCM	192	288	CanESM5	64	128
CNRM-CM6-1-HR	360	720	CAS-ESM2-0	128	256
E3SM-1-0	180	360	CESM2-FV2	96	144
E3SM-1-1-ECA	180	360	CESM2-WACCM-FV2	96	144
FIO-ESM-2-0	192	288	CNRM-CM6-1	128	256
GFDL-CM4	180	288	CNRM-ESM2-1	128	256
GFDL-ESM4	180	288	GISS-E2-1-G	90	144
MPI-ESM1-2-HR	192	384	GISS-E2-1-G-CC	90	144
MRI-ESM2-0	160	320	GISS-E2-1-H	90	144
NorESM2-MM	192	288	HadGEM3-GC31-L	144	192
			IPSL-CM6A-LR	143	144
			MIROC6	128	256
			MPI-ESM1-2-HAM	96	192
			MPI-ESM1-2-LR	96	192
			NorESM2-LM	96	144

low spatial resolution simulations (CNRM-CM6-1, MPI-ESM1-2, and NorESM2), confirming that any difference due to spatial resolution is minimal. For shallow soil moisture, therefore, it suggests that modeled output is influenced more by the model of the land–atmosphere interaction than by spatial resolution, at least in large-scale experiments.

Figure 8 illustrates the same evaluation as in Fig. 7, but for deep soil moisture. Compared with shallow soils, simulated deep soil moisture is consistent with the reanalysis in the Northern Hemisphere; most COR values between modeled and reanalysis data range from 0.30 to 0.85, and STD and RMSE values fall within the range 0.5–1.0. CMIP5-simulated deep soil moisture is also more closely aligned with reanalysis data than are simulated shallow soil values (Li et al. 2007). This phenomenon reflects the direct impact of precipitation, evaporation, and surface runoff, which make shallow soil moisture intrinsically more variable than deep soil moisture. Nonetheless, a direct comparison with the reanalysis data indicates that several CMIP6 models (BCC-CSM2-MR, BCC-ESM1, GISS-E2-1-G, GISS-E2-1-G-CC, and GISS-E2-1-H) produce a significant offset in the Northern Hemisphere, whereas others (CESM2, CESM2-FV2, CESM2-WACCM, CESM2-WACCM-FV2, IPSL-CM6A-LR, MIROC6, NorESM2-LM, and NorESM2-MM) produce little or no offset. In the Southern Hemisphere, the difference between model output and reanalysis data is relatively small: COR values typically fall between 0.60 and 0.95, and STD and RMSE values between 0.5 and 1.5. Similarly, simulated deep soil moisture does not appear to depend on model resolution. Overall, the CMIP6-MMEM performs better than the majority of single-model simulations in terms of COR, STD, and RMSE.

From the analysis described above, the difference between CMIP6-modeled shallow soil moisture and reanalysis data is relatively large in the Northern Hemisphere. To help identify the mechanisms behind this variability, the Northern Hemisphere is divided into discrete regions so as to

enable a more detailed evaluation. Figure 9a depicts shallow soil moisture Taylor diagrams for CMIP6 and ERA5 in the eight Northern Hemisphere regions (SIB, M-AS, TIB, L-AS, EUR, WNA, ENA, and NA-WA). It is immediately clear from this statistical treatment that large interregional differences exist. For example, although simulations in L-AS and EUR align closely with reanalysis data (COR values of 0.85–0.95; STD and RMSE values of <2.0), those for M-AS, ENA, and WNA exhibit noticeably lower COR values (0.50–0.75) and larger STD and RMSE values (<4.5), whereas simulations for the TIB, SIB, and NA-WA are generally poor. For instance, the SIB simulations not only exhibit low COR values, but they also return the highest STD and RMSE values (e.g., CESM2-WACCM, CESM2, E3SM-1-1-ECA, E3SM-1-0, NorESM2-LM, NorESM2-MM, and CanESM5 give STD and RMSE values between 6.0 and 8.0). In contrast, although the STD and RMSE values on the TIB and in NA-WA are not large, COR values for both regions are low. Moreover, there is significant disparity among models for the TIB and NA-WA, whereas other regions produce highly consistent simulations. However, the MMEM produces output for the TIB and NA-WA that is closer to the reanalysis data (COR = 0.48 and 0.70; STD = 0.33 and 0.76; RMSE = 0.89 and 0.72).

Regional Taylor diagrams for CMIP6- and GLDAS-derived Northern Hemisphere shallow soil moisture values are consistent with those of the CMIP6-ERA5 assessment (Fig. 9b). Simulations align well with the reanalysis data in L-AS, EUR, ENA, and WNA, whereas those for the TIB and NA-WA exhibit greater variability. In SIB, the relationship between CMIP6 model output and GLDAS data is greatly improved, with COR values of 0.60–0.85, and the reasons will be analyzed and discussed later.

For NA-WA, the soil moisture is always low due to the prevailing aridity. Therefore, even minor differences between CMIP6 models and the reanalysis data can result in poor

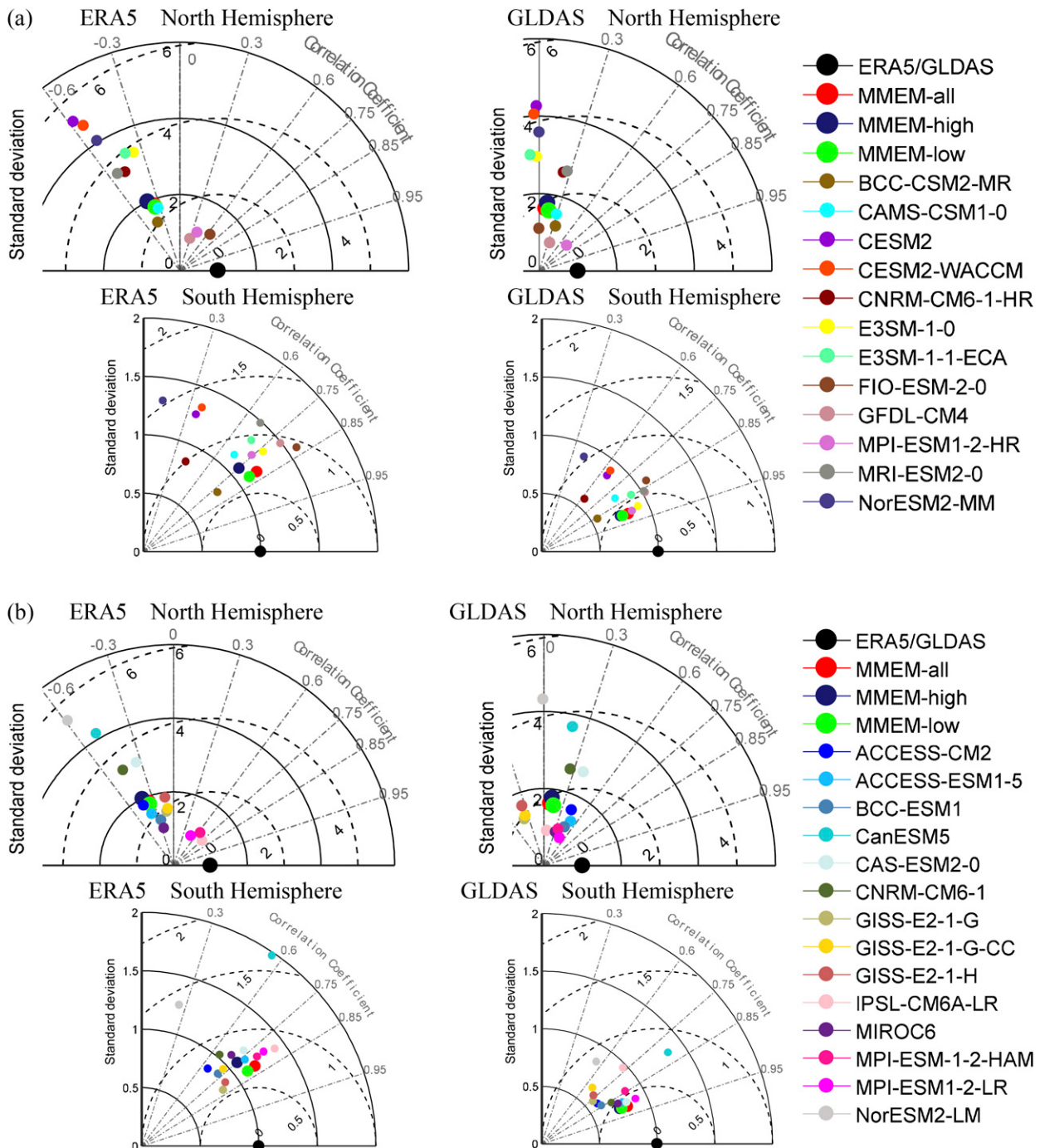


FIG. 7. Taylor diagram of shallow soil moisture output from the (a) high-resolution and (b) low-resolution model groups for temporal variability for (top) the Northern Hemisphere and (bottom) the Southern Hemisphere. CMIP6 model output is compared to (left) ERA5 and (right) GLDAS reanalysis data. The large red, dark blue, and green dots represent the CMIP6 models MMEM (MMEM-all) and the high-resolution MMEM (MMEM-high) and low-resolution MMEM (MMEM-low), respectively. The azimuthal angle represents the correlation coefficient (gray dotted line), the distance from origin (black solid line) represents model STD, and the distance from reanalysis data (black dashed line) indicates the RMSE (note that STD and RMSE are standardized).

COR values. Precipitation and evaporation simulations for NA-WA are also characterized by significant deviations (Figs. 4b–d), which is the reason for the poor simulation of

soil moisture. For both the TIB and SIB regions, the most significant difference between these and other regions is that they are considerably influenced by cold-season processes,

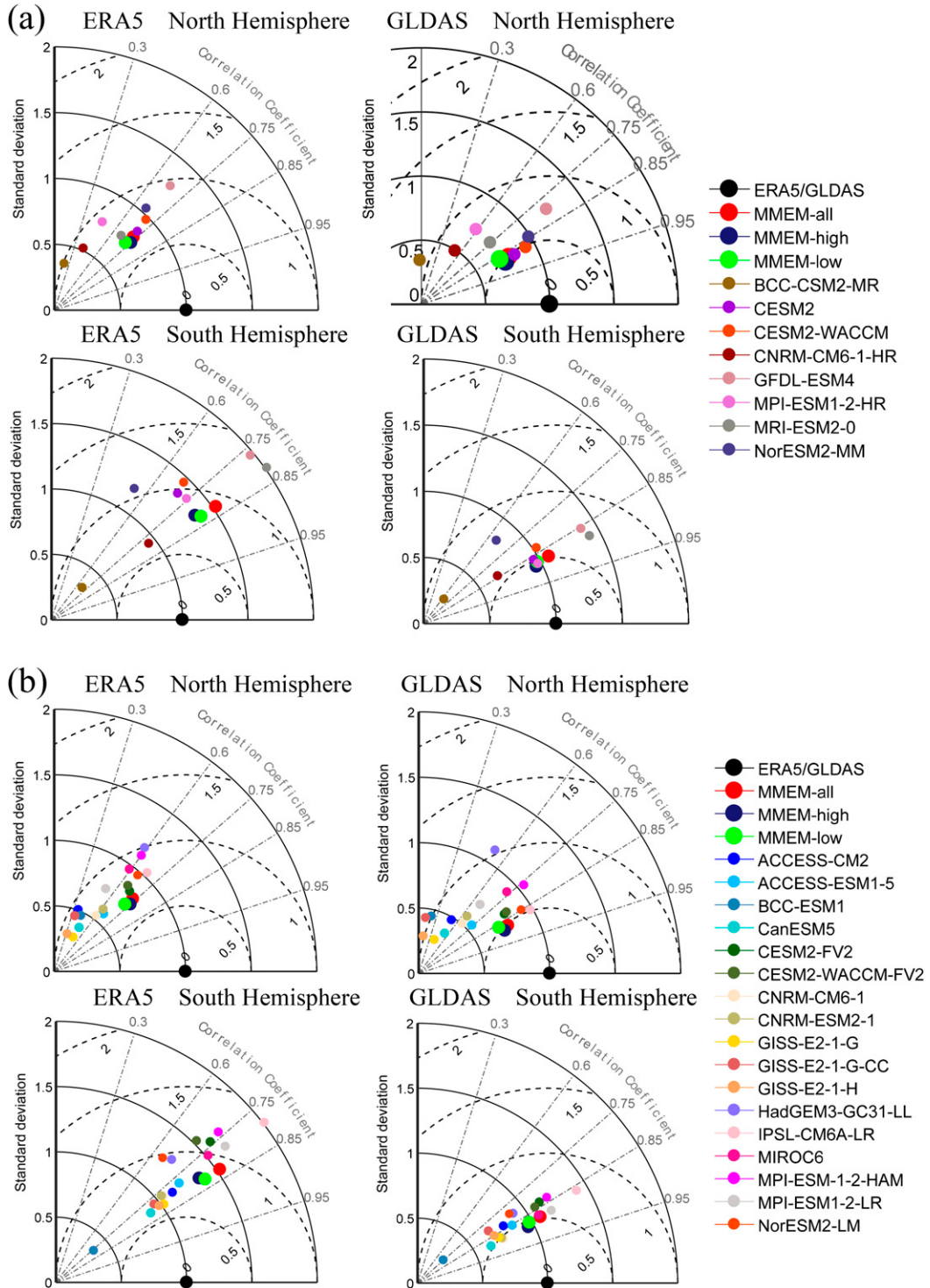


FIG. 8. As in Fig. 7, but for deep soil moisture.

such as snow cover, frozen soil, and their melting processes. However, the snow model often has notable uncertainties among the various models (Chen et al. 2013; Menard et al. 2021), potentially resulting in significant differences in soil

moisture simulations. For the analysis of simulation performance of shallow soil moisture in TIB and SIB, not only surface available water needs to be considered, but also the cold-season processes.

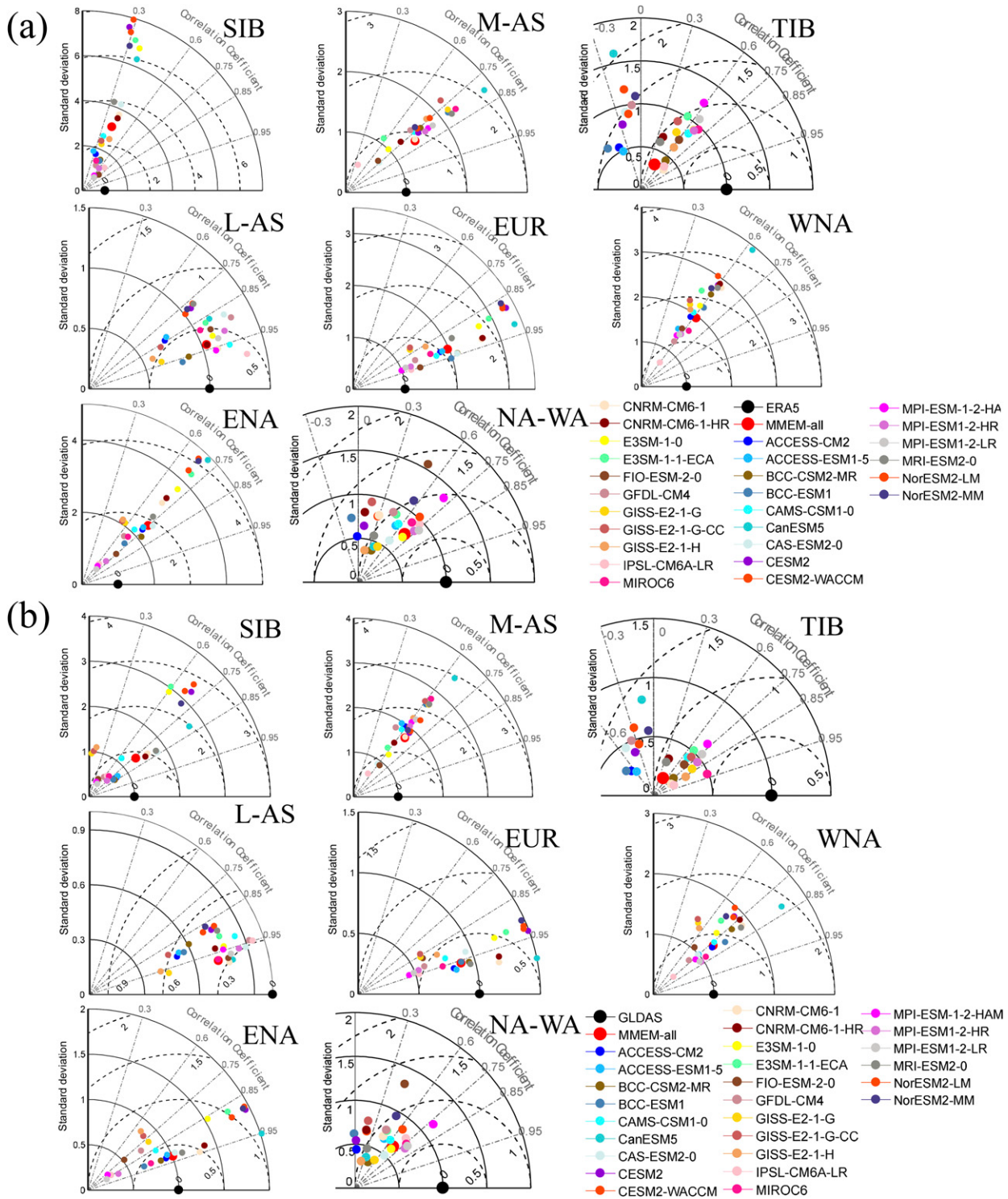


FIG. 9. Taylor diagram comparison of shallow soil moisture CMIP6 model output and (a) ERA5 and (b) GLDAS data for temporal variability in the Northern Hemisphere study regions (SIB, M-AS, TIB, L-AS, EUR, WNA, ENA, and NA-WA).

To this end, Fig. 10 shows Taylor diagrams for precipitation, evaporation, surface runoff, and snowmelt on the TIB and in SIB. For the TIB (Fig. 10a), the difference between

modeled and reanalysis precipitation and evaporation data is minimal. Nevertheless, the STD and RMSE for surface runoff are both large (ranging from 2.0 to 6.0) between GLDAS and

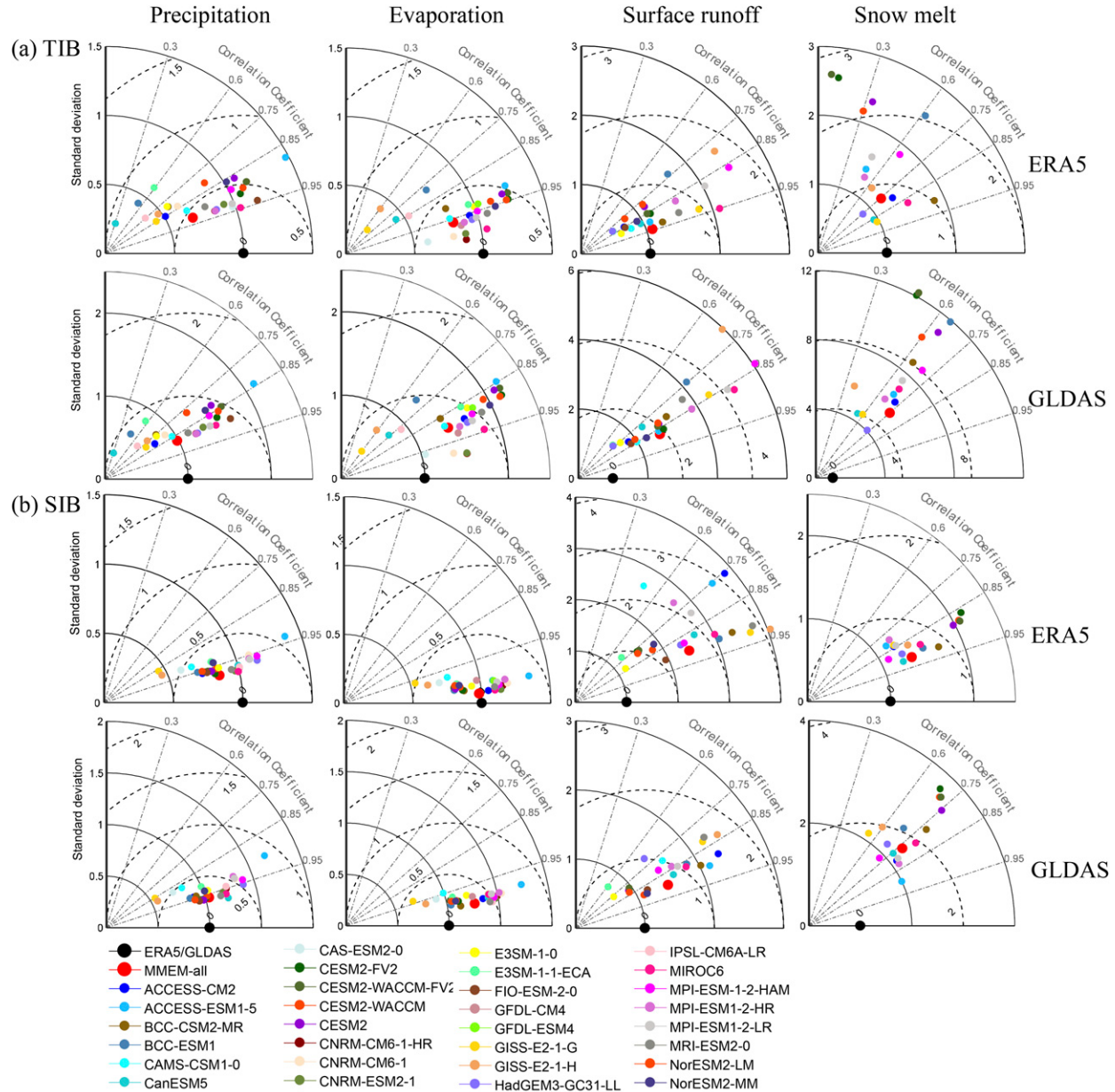


FIG. 10. Taylor diagram of (from left to right) precipitation, evaporation, surface runoff, and snowmelt for temporal variability over (a) TIB and (b) SIB (top) between ERA5 and CMIP6-MMEM and (bottom) between GLDAS and CMIP6-MMEM.

CMIP6. In terms of snowmelt, regardless of ERA5 or GLDAS, the models all exhibit considerable deviations. In the Taylor diagram, the COR values for ERA5 and CMIP6 are highly scattered and small (0.00–0.85), and the STD and RMSE values range from 1.0 to 3.0. Although COR values are higher (0.40–0.75) for GLDAS, the STD and RMSE values are worse (ranging from 4.0 to 12.0).

Both precipitation and evaporation are accurately reproduced by models for SIB and the TIB, which give similar values (Fig. 10b). Although simulated runoff and snowmelt are

not as accurate as the output for precipitation and evaporation, they are nonetheless improved relative to the TIB. COR values for surface runoff generally fall between 0.60 and 0.95, and STD and RMSE values range from 1.0 to 4.0. Overall, the offset between CMIP6 and ERA5 data is larger than that between CMIP6 and GLDAS. Yet, for snowmelt, the GLDAS deviation exceeds that of ERA5. Specifically, ERA5 gives COR values of 0.75–0.95, with STD and RMSE values of 1.0–2.2, whereas GLDAS gives COR values ranging from 0.60 to 0.85 and STD and RMSE values of 2.0–4.0. As

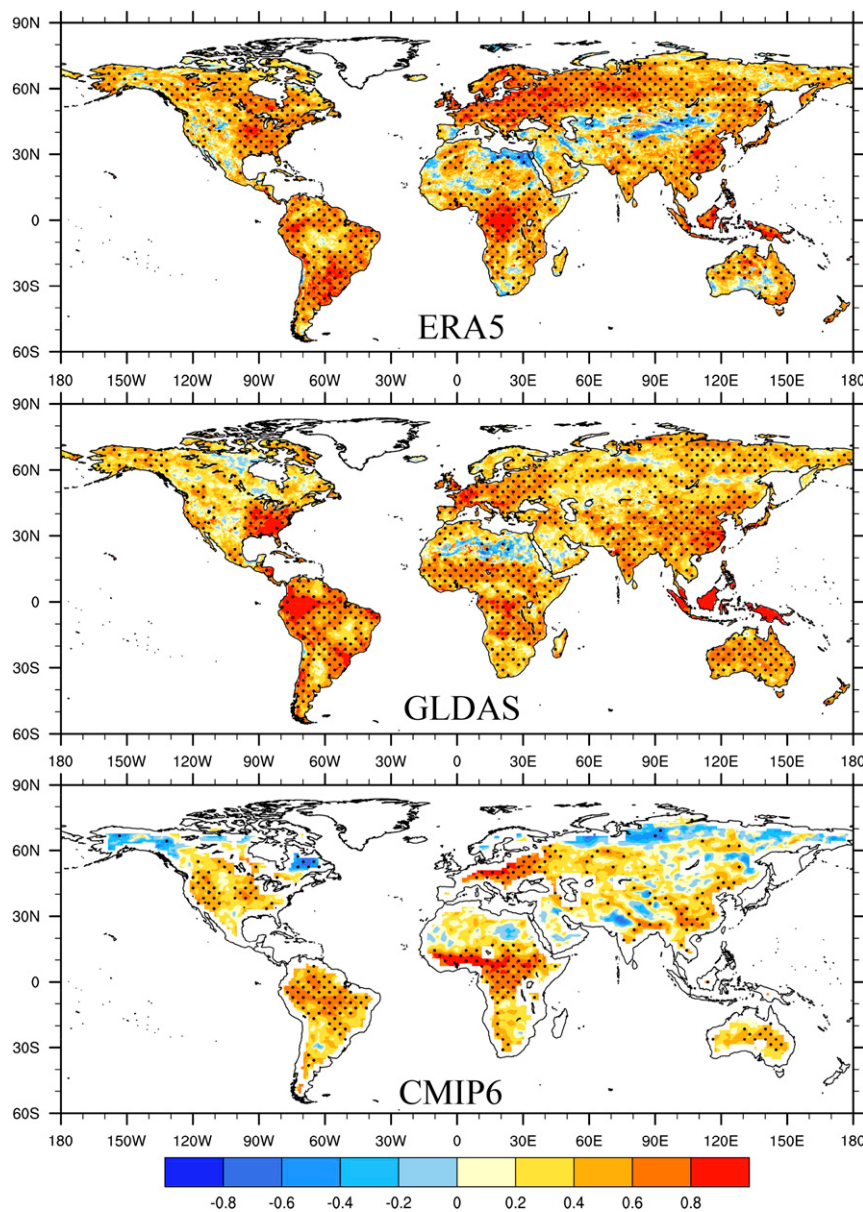


FIG. 11. Spatial distribution of the correlation (1979–2014, monthly data) between shallow soil moisture and $P - E$, for (top) ERA5, (middle) GLDAS, and (bottom) CMIP6-MMEM. Black dots indicate where a given area passes the 95% significance test.

depicted in the Taylor diagram of SIB soil moisture (Fig. 9), GLDAS is more closely aligned with the CMIP6-MMEM than with ERA5. Based on the above analysis, it suggests that surface runoff is better represented by GLDAS and the CMIP6-MMEM than by ERA5. This result is supported by the analysis of $P - E - R$ (Figs. 4b,d), in which the $P - E - R$ bias for SIB is smaller using the GLDAS dataset than it is with ERA5 data. Ultimately, these findings suggest that the offset in shallow soil

moisture between CMIP6 models and reanalysis data is potentially due to the effects of runoff and snowmelt over the TIB and SIB.

The analysis described above demonstrates that, despite the minor offset in precipitation and evaporation between the models and reanalysis, soil moisture may nonetheless be impacted by non-precipitation-related cold-season processes in high-altitude and/or high-latitude areas. These processes can result in significant deviation between modeled

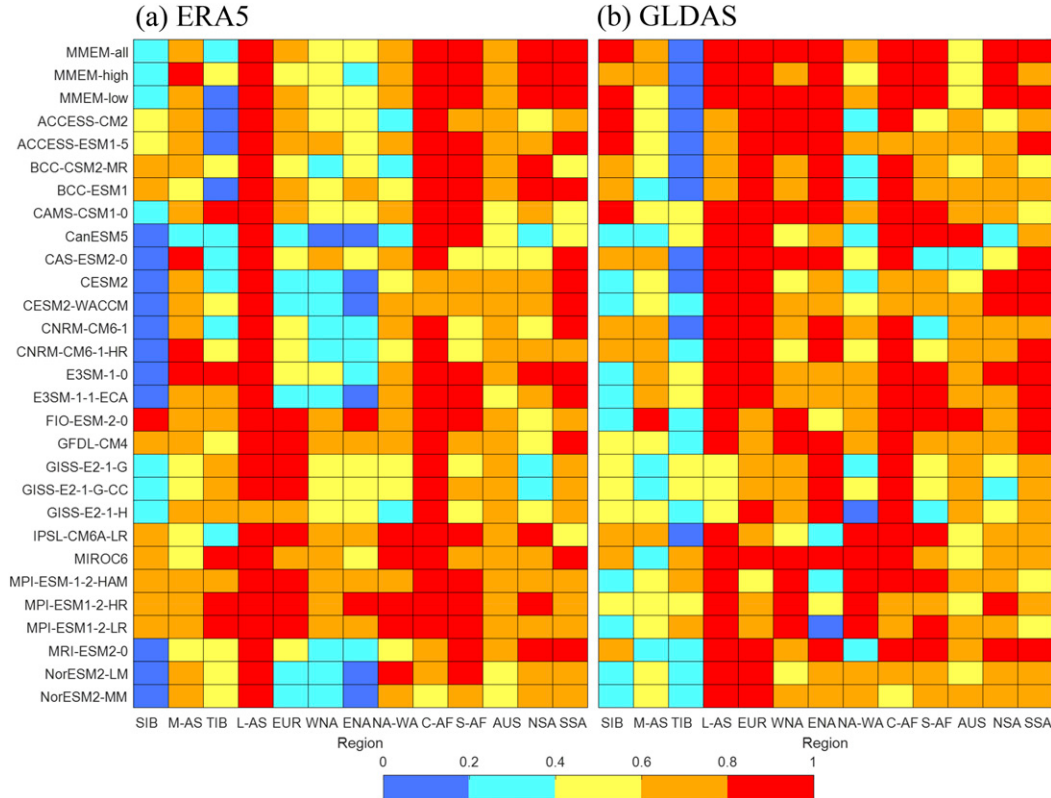


FIG. 12. Comparison of TSS between CMIP6 model output and (a) ERA5 and (b) GLDAS data for shallow soil moisture in each region. The horizontal and vertical axes represent regions and models, respectively. The grid color denotes TSS value.

and reanalysis values. To investigate this possibility in greater detail, the spatial distribution of the COR between $P - E$ and shallow soil moisture among the various datasets is analyzed (Fig. 11). For ERA5 and GLDAS, most regions are dominated by significantly positive values, with the exception of several minor areas in NA-WA and M-AS that exhibit weakly negative COR values. In contrast, the CMIP6-MMEM returns large-scale, negative COR values for SIB, the TIB, Alaska, and the Labrador Peninsula, all of which are severely impacted by cold-season dynamics. This pattern agrees with the previous analysis of SIB and TIB. Although CMIP6 models can simulate precipitation and evaporation effectively, soil moisture in these areas is also dominated by the seasonal expansion and thaw of snow cover and frozen soil, which combine to exert a large impact on soil moisture on the TIB and at high latitudes (Shinoda 2001; Luo et al. 2003; Chang et al. 2014). Specifically, these cold-season processes can retain and release large volumes of nonprecipitable water to the soil moisture budget, resulting in a poor correlation.

In ERA5 and GLDAS, however, soil moisture and $P - E$ nonetheless maintain good correlations for the TIB and high latitudes, indicating that the soil moisture incorporated in reanalysis datasets is dominated by precipitation and

evaporation, with little contribution from cold-season processes. This outcome implies that the significant discrepancy between reanalysis data and CMIP6 in SIB and TIB derives not from inferior modeling capabilities within CMIP6, but from the limitations of reanalysis data in regions affected by cold-season processes. Concurrently, a number of arid regions (NA-WA, M-AS, etc.) also exhibit weakly negative or weakly positive COR values, or failed the significance test. This poor performance is due to the inherently low soil moisture and $P - E$ values in arid environments, in which even minor disturbances serve to weaken the COR.

To quantify the effect on simulation output of using different CMIP6 models for each region, TSS analysis is used for the evaluation. Figure 12 shows the comparison of TSS between regional CMIP6 model output and reanalysis data for shallow soil moisture. Compared with ERA5, the majority of CMIP6 models exhibit higher TSS values with GLDAS data, particularly in EUR, WNA, and ENA. For both ERA5 and GLDAS, TSS values are very high in L-AS and the Southern Hemisphere, but relatively low in SIB and the TIB.

TSS analysis is also performed on deep soil moisture (Fig. 13). Compared with the shallow results, and consistent with the previous analysis, TSS values for deep soil moisture are improved both for the SIB and TIB regions

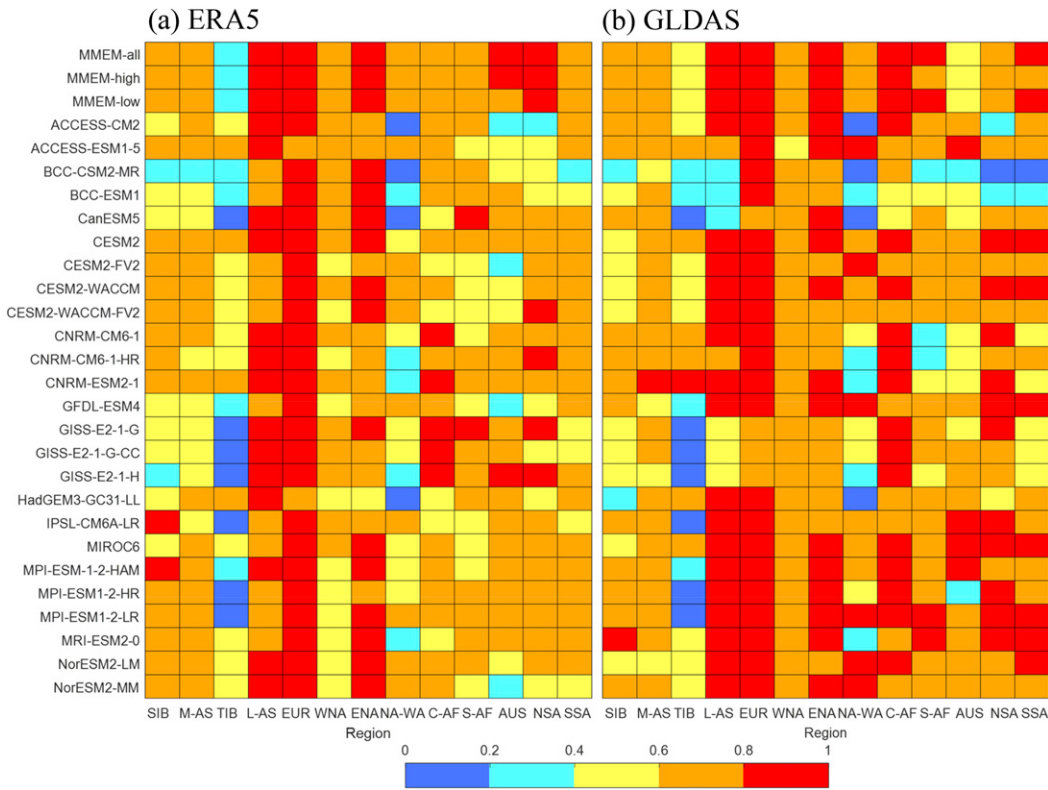


FIG. 13. As in Fig. 10, but for deep soil moisture.

(Figs. 7 and 8). Similar to shallow soil moisture, TSS values are generally higher in L-AS, EUR, WNA, ENA, and the Southern Hemisphere, and only a few models return relatively low values for the TIB and NA-WA.

For the purpose of quantifying and comparing model efficacy, we statistically assessed the TSS values of various models simulating conditions in different regions. When the TSS value is close to 1, this indicates that values of COR and STD in CMIP6 output agree with reanalysis datasets. When the TSS value exceeds 0.6, it indicates that the model can reproduce the climatological soil moisture distribution effectively (Taylor 2001; Yuan and Quiring 2017). Therefore, to compare the TSS of different models and regions more thoroughly, we counted the number of models with $TSS > 0.6$ by region (Fig. 14a) and the number of regions with $TSS > 0.6$ by model (Fig. 14b).

In relation to the region (Fig. 14a), the majority of shallow soil moisture simulations align with reanalysis data in most regions evaluated, yet diverge markedly on the TIB and in SIB and M-AS. Similarly, simulations of deep soil moisture align well with the reanalysis data generally but deviate largely on the TIB and in SIB and NA-WA. These results are consistent with the previous analysis of the precipitation, evaporation, and surface available water ratios of bias (Fig. 4), Taylor diagrams (Figs. 7–10), and distributions of COR between $P - E$ and soil moisture (Fig. 11).

In relation to the model (Fig. 14b), the top-five best-performing models (which produced the smallest offsets with reanalysis data for shallow soil moisture) as FIO-ESM-2-0, MPI-ESM1-2-LR, MIROC6, ACCESS-ESM1-5, and GFDL-CM4. Correspondingly, the best-performing land models are CLM, JSBACH, MATSIRO, CABLE, and LM4.0 (Table 1). The greatest disparities in simulated output arise from models CanESM5, GISS-E2-1-G, GISS-E2-1-H, and GISS-E2-1-G-CC. For deep soil moisture, the top-five best-performing models are CESM2, MPI-ESM1-2-LR, ACCESS-ESM1-5, CESM2-WACCM, and CNRM-ESM2-1, and the most effective land models are CLM, JSBACH, CABLE, and ISBA (Table 1). In contrast, the models BCC-CSM2-MR and BCC-ESM1 produce the largest offsets. For shallow soil moisture simulation, the reason for the poor simulation of CanESM5 model is caused by its quite different from ERA5. Similarly, The GISS model simulation differs greatly from reanalysis data because the GISS model and reanalysis data are quite different in NSA, North America, and S-AF.

4. Discussion and summary

This study evaluated CMIP6 simulations of shallow and deep soil moisture via comparison of model output with

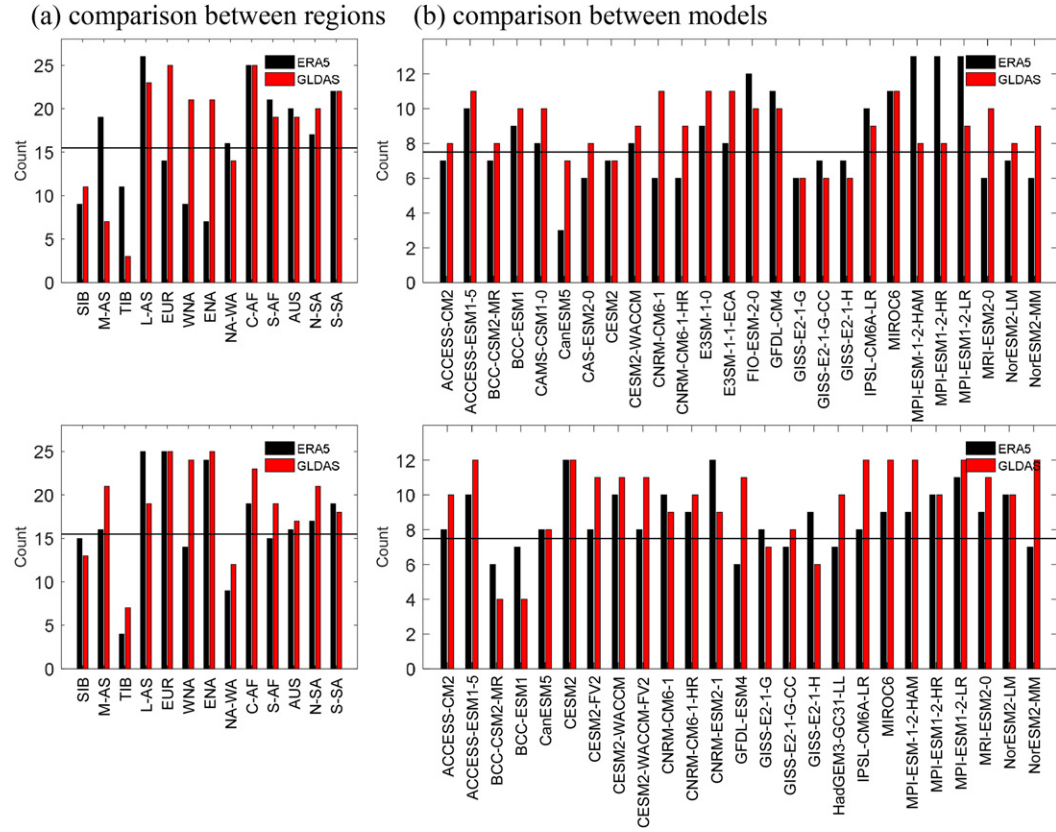


FIG. 14. (a) Statistics for the number of models with $TSS > 0.6$, displayed by region. (b) Statistics for the number of regions with $TSS > 0.6$, displayed by model. Results are for (top) shallow soil moisture and (bottom) deep soil moisture. The black bar represents ERA5, and the red bar represents GLDAS.

ERA-Interim, ERA5, and GLDAS data. The assessment confirms that the CMIP6-MMEM is a more effective means for reproducing the climatology, spatial distribution, and annual cycle characteristics of soil moisture than most single-model simulations. This outcome is attributed to the capacity of the MMEM to filter out uncertainties arising from model differences and initial conditions. For shallow and deep soil moisture, the typically arid and humid regions correspond to the dry and wet centers of soil moisture as depicted by reanalysis datasets and CMIP6-MMEM output. For example, there are dry centers of soil moisture in NA-WA, and S-AF, whereas there are wet centers of soil moisture in the high latitudes of the Northern Hemisphere, southeastern China, and NSA. Overall, the bias between CMIP6-MMEM and reanalysis data is minor in the Southern Hemisphere and low-latitude Northern Hemisphere, whereas the CMIP6-MMEM simulated higher soil moisture values relative to the reanalysis over mid- to high northern latitudes and high mountains. The majority of CMIP6 models can effectively simulate seasonal variations in shallow soil moisture, such as the annual peaks in the thawing season over the mid- to high latitudes and in the rainy season over the low latitudes. Consequently, the range of the MMEM annual cycle also aligns well with

reanalysis data. The comparison of high- and low-spatial resolution soil moisture simulations revealed no significant difference between the two groups, indicating that improved spatial resolution is not currently the limiting factor for simulating soil moisture.

In most CMIP6 models, simulated shallow soil moisture aligns with reanalysis data in EUR, L-AS, and the Southern Hemisphere, but diverges from the reanalysis on the TIB and in NA-WA and SIB. Over the hyper-arid NA-WA, where soil moisture values are inherently low, fluctuations due to precipitation can be relatively extreme, a characteristic common to all arid areas evaluated here. Over the TIB and in SIB, simulations of soil moisture are complicated by the limited capacity of models to incorporate cold-season processes. Concurrently, the dearth of information on these specific processes also impacts the ability of reanalysis to represent soil moisture accurately. Therefore, the disagreement between CMIP6 and reanalysis datasets in areas subject to extreme wintertime cooling is not strictly due to imperfections within the CMIP6 models alone. Instead, we propose that the offset also reflects limitations within the reanalysis datasets.

This evaluation underscores the minimal disparity in soil moisture between CMIP6 simulations and reanalysis data in

the Southern Hemisphere, which we suggest reflects the relatively minor influence of cold-season processes in the Southern Hemisphere (excluding the Antarctic) compared with the Northern Hemisphere. Alternatively, the close agreement might be due to the scarcity of observation sites in the Southern Hemisphere, since reanalysis data will be affected less by the observational data and more by the model, resulting in a similar fit between the two. Therefore, it is critically important that the accuracy of the dataset used to evaluate model performance is first verified (Collins et al. 2013). Similarly, CMIP6 simulations of deep soil moisture are generally in accord with the reanalysis data when viewed as a global average, potentially as a consequence of the slight changes in deep soil moisture and dominance of simulated output over reanalyzed values. Although there are great differences in value range of soil moisture simulation among different models, the simulated temporal variation is more critical to the simulation performance of soil moisture (Koster et al. 2009). In our analysis, most models can reproduce the annual cycle characteristics of soil moisture well. Ultimately, we conclude that FIO-ESM2-0, MPI-ESM1-2-LR, MIROC6, ACCESS-ESM1-5, and GFDL-CM4 are the top-five best-performing models for reconstructing and projecting shallow soil moisture, and CESM2, MPI-ESM1-2-LR, ACCESS-ESM1-5, CESM2-WACCM, and CNRM-ESM2-1 are the top-five most effective for evaluating deep soil moisture.

Acknowledgments. This study was jointly funded by the National Key Research and Development Program (2016YFA0601502) and National Natural Science Foundation of China (41822503, 41375092, and 42005056).

ERA-Interim and ERA5 datasets during this study are openly available from the European Centre for Medium-Range Weather Forecasts at <https://www.ecmwf.int/en/forecasts/datasets/reanalysis-datasets/era-interim> and <https://cds.climate.copernicus.eu/cdsapp#!/search?type=dataset>. GLDAS-NOAH 2.0 reanalysis datasets during this study are openly available from the National Aeronautics and Space Administration at <https://disc.gsfc.nasa.gov/datasets?keywords=GLDAS>. CMIP6 data during this study are openly available from the World Climate Research Programme at <https://esgf-node.llnl.gov/search/cmip6/>.

REFERENCES

- Albergel, C., P. de Rosnay, G. Balsamo, L. Isaksen, and J. Muñoz-Sabater, 2012: Soil moisture analyses at ECMWF: Evaluation using global ground-based in situ observations. *J. Hydrometeor.*, **13**, 1442–1460, <https://doi.org/10.1175/JHM-D-11-0107.1>.
- Berg, A., J. Sheffield, and P. C. D. Milly, 2017: Divergent surface and total soil moisture projections under global warming. *Geophys. Res. Lett.*, **44**, 236–244, <https://doi.org/10.1002/2016GL071921>.
- Bi, H., J. Ma, W. Zheng, and J. Zeng, 2016: Comparison of soil moisture in GLDAS model simulations and in situ observations over the Tibetan Plateau. *J. Geophys. Res. Atmos.*, **121**, 2658–2678, <https://doi.org/10.1002/2015JD024131>.
- Bosilovich, M. G., and J. Chern, 2006: Simulation of water sources and precipitation recycling for the MacKenzie, Mississippi, and Amazon River basins. *J. Hydrometeor.*, **7**, 312–329, <https://doi.org/10.1175/JHM501.1>.
- Brubaker, K. L., D. Entekhabi, and P. Eagleson, 1993: Estimation of continental precipitation recycling. *J. Climate*, **6**, 1077–1089, [https://doi.org/10.1175/1520-0442\(1993\)006<1077:EOCPR>2.0.CO;2](https://doi.org/10.1175/1520-0442(1993)006<1077:EOCPR>2.0.CO;2).
- Chang, J., G. Wang, Y. Gao, and Y. Wang, 2014: The influence of seasonal snow on soil thermal and water dynamics under different vegetation covers in a permafrost region. *J. Mt. Sci.*, **11**, 727–745, <https://doi.org/10.1007/s11629-013-2893-0>.
- Chen, Y., K. Yang, J. Qin, L. Zhao, W. Tang, and M. Han, 2013: Evaluation of AMSR-E retrievals and GLDAS simulations against observations of a soil moisture network on the central Tibetan Plateau. *J. Geophys. Res. Atmos.*, **118**, 4466–4475, <https://doi.org/10.1002/jgrd.50301>.
- Cheng, M., L. Zhong, Y. Ma, M. Zou, N. Ge, X. Wang, and Y. Hu, 2019: A study on the assessment of multi-source satellite soil moisture products and reanalysis data for the Tibetan Plateau. *Remote Sens.*, **11**, 1196, <https://doi.org/10.3390/rs11101196>.
- Clark, M. P., and Coauthors, 2015: Improving the representation of hydrologic processes in Earth system models. *Water Resour. Res.*, **51**, 5929–5956, <https://doi.org/10.1002/2015WR017096>.
- Collins, M., K. AchutaRao, K. Ashok, S. Bhandari, A. Mitra, S. Prakash, R. Srivastava, and A. Turner, 2013: Observational challenges in evaluating climate models. *Nat. Climate Change*, **3**, 940–941, <https://doi.org/10.1038/nclimate2012>.
- Delworth, T., and S. Manabe, 1988: The influence of potential evaporation on the variabilities of simulated soil wetness and climate. *J. Climate*, **1**, 523–547, [https://doi.org/10.1175/1520-0442\(1988\)001<0523:TIOPEO>2.0.CO;2](https://doi.org/10.1175/1520-0442(1988)001<0523:TIOPEO>2.0.CO;2).
- Deng, M., and Coauthors, 2020: Responses of soil moisture to regional climate change over the Three Rivers Source Region on the Tibetan Plateau. *Int. J. Climatol.*, **40**, 2403–2417, <https://doi.org/10.1002/joc.6341>.
- Douville, H., 2002: Influence of soil moisture on the Asian and African monsoons. Part II: Interannual variability. *J. Climate*, **15**, 701–720, [https://doi.org/10.1175/1520-0442\(2002\)015<0701:IOSMOT>2.0.CO;2](https://doi.org/10.1175/1520-0442(2002)015<0701:IOSMOT>2.0.CO;2).
- , F. Chauvin, and H. Broqua, 2001: Influence of soil moisture on the Asian and African monsoons. Part I: Mean monsoon and daily precipitation. *J. Climate*, **14**, 2381–2403, [https://doi.org/10.1175/1520-0442\(2001\)014<2381:IOSMOT>2.0.CO;2](https://doi.org/10.1175/1520-0442(2001)014<2381:IOSMOT>2.0.CO;2).
- Eltahir, E., and R. Bras, 1996: Precipitation recycling. *Rev. Geophys.*, **34**, 367–378, <https://doi.org/10.1029/96RG01927>.
- Eyring, V., S. Bony, G. Meehl, C. Senior, B. Stevens, R. Stouffer, and K. Taylor, 2016: Overview of the Coupled Model Inter-comparison Project phase 6 (CMIP6) experimental design and organization. *Geosci. Model Dev.*, **9**, 1937–1958, <https://doi.org/10.5194/gmd-9-1937-2016>.
- Findell, K., and E. Eltahir, 2003: Atmospheric controls on soil moisture-boundary layer interactions. Part II: Feedbacks within the continental United States. *J. Hydrometeor.*, **4**, 570–583, [https://doi.org/10.1175/1525-7541\(2003\)004<0570:ACOSML>2.0.CO;2](https://doi.org/10.1175/1525-7541(2003)004<0570:ACOSML>2.0.CO;2).
- Fischer, E., S. Seneviratne, P. Vidale, D. Lüthi, and C. Schär, 2007: Soil moisture–atmosphere interactions during the 2003 European summer heat wave. *J. Climate*, **20**, 5081–5099, <https://doi.org/10.1175/JCLI4288.1>.
- Ford, T., and S. Quiring, 2014: In situ soil moisture coupled with extreme temperatures: A study based on the Oklahoma Mesonet. *Geophys. Res. Lett.*, **41**, 4727–4734, <https://doi.org/10.1002/2014GL060949>.
- Fu, S., S. Nie, Y. Luo, and X. Chen, 2020: Implications of diurnal variations in land surface temperature to data assimilation

- using MODIS LST data. *J. Geogr. Sci.*, **30**, 18–36, <https://doi.org/10.1007/s11442-020-1712-0>.
- Gleckler, P. J., K. E. Taylor, and C. Doutriaux, 2008: Performance metrics for climate models. *J. Geophys. Res.*, **113**, D06104, <https://doi.org/10.1029/2007JD008972>.
- Greve, P., B. Orlowsky, B. Mueller, J. Sheffield, M. Reichstein, and S. I. Seneviratne, 2014: Global assessment of trends in wetting and drying over land. *Nat. Geosci.*, **7**, 716–721, <https://doi.org/10.1038/ngeo2247>.
- Hagemann, S., and T. Stacke, 2015: Impact of the soil hydrology scheme on simulated soil moisture memory. *Climate Dyn.*, **44**, 1731–1750, <https://doi.org/10.1007/s00382-014-2221-6>.
- Hauser, M., R. Orth, and S. I. Seneviratne, 2016: Role of soil moisture versus recent climate change for the 2010 heat wave in western Russia. *Geophys. Res. Lett.*, **43**, 2819–2826, <https://doi.org/10.1002/2016GL068036>.
- Hersbach, H., and Coauthors, 2020: The ERA5 global reanalysis. *Quart. J. Roy. Meteor. Soc.*, **146**, 1999–2049, <https://doi.org/10.1002/qj.3803>.
- Hirschi, M., and Coauthors, 2011: Observational evidence for soil moisture impact on hot extremes in southeastern Europe. *Nat. Geosci.*, **4**, 17–21, <https://doi.org/10.1038/ngeo1032>.
- Jamison, N., and S. Kravtsov, 2010: Decadal variations of North Atlantic sea surface temperature in observations and CMIP3 simulations. *J. Climate*, **23**, 4619–4636, <https://doi.org/10.1175/2010JCLI3598.1>.
- Koster, R. D., and M. J. Suarez, 2001: Soil moisture memory in climate models. *J. Hydrometeor.*, **2**, 558–570, [https://doi.org/10.1175/1525-7541\(2001\)002<0558:SMMC>2.0.CO;2](https://doi.org/10.1175/1525-7541(2001)002<0558:SMMC>2.0.CO;2).
- , Z. Guo, R. Yang, P. A. Dirmeyer, K. Mitchell, and M. J. Puma, 2009: On the nature of soil moisture in land surface models. *J. Climate*, **22**, 4322–4335, <https://doi.org/10.1175/2009JCLI2832.1>.
- Li, H., A. Robock, and M. Wild, 2007: Evaluation of Intergovernmental Panel on Climate Change Fourth Assessment soil moisture simulations for the second half of the twentieth century. *J. Geophys. Res.*, **112**, D05108, <https://doi.org/10.1029/2006JD007455>.
- Li, R., C. Wang, and D. Wu, 2016: Changes in precipitation recycling over arid regions in the Northern Hemisphere. *Theor. Appl. Climatol.*, **131**, 489–502, <https://doi.org/10.1007/s00704-016-1978-4>.
- Liu, L., R. Zhang, and Z. Zuo, 2014: Intercomparison of spring soil moisture among multiple reanalysis data sets over eastern China. *J. Geophys. Res. Atmos.*, **119**, 54–64, <https://doi.org/10.1002/2013JD020940>.
- , —, and —, 2017: Effect of spring precipitation on summer precipitation in eastern China: Role of soil moisture. *J. Climate*, **30**, 9183–9194, <https://doi.org/10.1175/JCLI-D-17-0028.1>.
- Lu, C., M. Kanamitsu, J. O. Roads, W. Ebisuzaki, K. E. Mitchell, and D. Lohmann, 2005: Evaluation of soil moisture in the NCEP–NCAR and NCEP–DOE global reanalyses. *J. Hydrometeor.*, **6**, 391–408, <https://doi.org/10.1175/JHM427.1>.
- Luo, L., and Coauthors, 2003: Effects of frozen soil on soil temperature, spring infiltration, and runoff: Results from the PILPS 2(d) experiment at Valdai, Russia. *J. Hydrometeor.*, **4**, 334–351, [https://doi.org/10.1175/1525-7541\(2003\)4<334:EOFSSO>2.0.CO;2](https://doi.org/10.1175/1525-7541(2003)4<334:EOFSSO>2.0.CO;2).
- Mahfouf, J. F., 1991: Analysis of soil moisture from near-surface parameters: A feasibility study. *J. Appl. Meteor.*, **30**, 1534–1547, [https://doi.org/10.1175/1520-0450\(1991\)030<1534:AOSMFN>2.0.CO;2](https://doi.org/10.1175/1520-0450(1991)030<1534:AOSMFN>2.0.CO;2).
- Menard, C. B., and Coauthors, 2021: Scientific and human errors in a snow model intercomparison. *Bull. Amer. Meteor. Soc.*, **102**, E61–E79, <https://doi.org/10.1175/BAMS-D-19-0329.1>.
- Mueller, B., and S. I. Seneviratne, 2014: Systematic land climate and evapotranspiration biases in CMIP5 simulations. *Geophys. Res. Lett.*, **41**, 128–134, <https://doi.org/10.1002/2013GL058055>.
- Nakaegawa, T., 2017: Statistical evaluation of future soil moisture changes in East Asia projected in a CMIP5 multi-model ensemble. *Hydrol. Res. Lett.*, **11**, 37–43, <https://doi.org/10.3178/hr.11.37>.
- Orth, R., and S. I. Seneviratne, 2012: Analysis of soil moisture memory from observations in Europe. *J. Geophys. Res.*, **117**, D15115, <https://doi.org/10.1029/2011JD017366>.
- , and —, 2014: Using soil moisture forecasts for sub-seasonal summer temperature predictions in Europe. *Climate Dyn.*, **43**, 3403–3418, <https://doi.org/10.1007/s00382-014-2112-x>.
- Peng, J., J. Niesel, A. Loew, S. Zhang, and J. Wang, 2015: Evaluation of satellite and reanalysis soil moisture products over southwest China using ground-based measurements. *Remote Sens.*, **7**, 15 729–15 747, <https://doi.org/10.3390/rs71115729>.
- Santanello, J. A., C. D. Peters-Lidard, S. V. Kumar, C. Alonge, and W. Tao, 2009: A modeling and observational framework for diagnosing local land–atmosphere coupling on diurnal time scales. *J. Hydrometeor.*, **10**, 577–599, <https://doi.org/10.1175/2009JHM1066.1>.
- Seneviratne, S. I., and Coauthors, 2006: Soil moisture memory in AGCM simulations: Analysis of Global Land–Atmosphere Coupling Experiment (GLACE) data. *J. Hydrometeor.*, **7**, 1090–1112, <https://doi.org/10.1175/JHM533.1>.
- , C. Thierry, L. Edouard, H. Martin, B. Eric, L. Irene, O. Boris, and J. Adriaan, 2010: Investigating soil moisture–climate interactions in a changing climate: A review. *Earth Sci. Rev.*, **99**, 125–161, <https://doi.org/10.1016/j.earscirev.2010.02.004>.
- Seo, E., and Coauthors, 2019: Impact of soil moisture initialization on boreal summer subseasonal forecasts: Mid-latitude surface air temperature and heat wave events. *Climate Dyn.*, **52**, 1695–1709, <https://doi.org/10.1007/s00382-018-4221-4>.
- Shinoda, M., 2001: Climate memory of snow mass as soil moisture over central Eurasia. *J. Geophys. Res.*, **106**, 33 393–33 403, <https://doi.org/10.1029/2001JD000525>.
- Taylor, K. E., 2001: Summarizing multiple aspects of model performance in a single diagram. *J. Geophys. Res.*, **106**, 7183–7192, <https://doi.org/10.1029/2000JD900719>.
- , R. J. Stouffer, and G. A. Meehl, 2012: An overview of CMIP5 and the experiment design. *Bull. Amer. Meteor. Soc.*, **93**, 485–498, <https://doi.org/10.1175/BAMS-D-11-00094.1>.
- van den Hurk, B., H. Kim, and G. Krinner, 2016: LS3MIP (v1.0) contribution to CMIP6: The Land Surface, Snow and Soil Moisture Model Intercomparison Project—Aims, setup and expected outcome. *Geosci. Model Dev.*, **9**, 2809–2832, <https://doi.org/10.5194/gmd-9-2809-2016>.
- Whan, K., J. Zscheischler, R. Orth, M. Shongwe, M. Rahimi, and E. O. Asare, and S. I. Seneviratne, 2015: Impact of soil moisture on extreme maximum temperatures in Europe. *Wea. Climate Extremes*, **9**, 57–67, <https://doi.org/10.1016/j.wace.2015.05.001>.
- Wu, W., and R. E. Dickinson, 2004: Time scales of layered soil moisture memory in the context of land–atmosphere interaction. *J. Climate*, **17**, 2752–2764, [https://doi.org/10.1175/1520-0442\(2004\)017<2752:TSOLSM>2.0.CO;2](https://doi.org/10.1175/1520-0442(2004)017<2752:TSOLSM>2.0.CO;2).
- , M. A. Geller, and R. E. Dickinson, 2002: The response of soil moisture to long-term variability of precipitation.

- J. Hydrometeor.*, **3**, 604–613, [https://doi.org/10.1175/1525-7541\(2002\)003<0604:TROSMT>2.0.CO;2](https://doi.org/10.1175/1525-7541(2002)003<0604:TROSMT>2.0.CO;2).
- Wu, Z., H. Feng, H. He, J. Zhou, and Y. Zhang, 2021: Evaluation of soil moisture climatology and anomaly components derived from ERA5-land and GLDAS-2.1 in China. *Water Resour. Manage.*, **35**, 629–643, <https://doi.org/10.1007/s11269-020-02743-w>.
- Yeh, T. C., R. T. Wetherald, and S. Manabe, 1984: The effect of soil moisture on the short-term climate and hydrology change—A numerical experiment. *Mon. Wea. Rev.*, **112**, 474–490, [https://doi.org/10.1175/1520-0493\(1984\)112<0474:TEOSMO>2.0.CO;2](https://doi.org/10.1175/1520-0493(1984)112<0474:TEOSMO>2.0.CO;2).
- Yuan, S., and S. M. Quiring, 2017: Evaluation of soil moisture in CMIP5 simulations over the contiguous United States using in situ and satellite observations. *Hydrol. Earth Syst. Sci.*, **21**, 2203–2218, <https://doi.org/10.5194/hess-21-2203-2017>.
- Zampieri, M., E. Serpetzoglou, E. N. Anagnostou, E. I. Nikopoulos, and A. Papadopoulos, 2012: Improving the representation of river–groundwater interactions in land surface modeling at the regional scale: Observational evidence and parameterization applied in the Community Land Model. *J. Hydrol.*, **420–421**, 72–86, <https://doi.org/10.1016/j.jhydrol.2011.11.041>.
- Zhang, G., J. Li, X. Rong, Y. Xin, J. Li, H. Chen, J. Su, and L. Hua, 2018: An assessment of CAMS-CSM in simulating land–atmosphere heat and water exchanges. *J. Meteor. Res.*, **32**, 862–880, <https://doi.org/10.1007/s13351-018-8055-0>.
- Zhang, J., Z. Yang, L. Wu, and K. Yang, 2019: Summer high temperature extremes over northeastern China predicted by spring soil moisture. *Sci. Rep.*, **9**, 12577, <https://doi.org/10.1038/s41598-019-49053-9>.
- Zhang, Q., S. Wang, F. Yang, P. Yue, T. Yao, and W. Wang, 2015: Characteristics of dew formation and distribution, and its contribution to the surface water budget in a semi-arid region in China. *Bound.-Layer Meteor.*, **154**, 317–331, <https://doi.org/10.1007/s10546-014-9971-x>.
- Zhang, R., and Z. Zuo, 2011: Impact of spring soil moisture on surface energy balance and summer monsoon circulation over East Asia and precipitation in east China. *J. Climate*, **24**, 3309–3322, <https://doi.org/10.1175/2011JCLI4084.1>.
- , L. Liu, and Z. Zuo, 2016: Variation of soil moisture over China and their influences on Chinese climate. *Chin. J. Nat.*, **38**, 313–319.
- Zhao, M., H. Zhang, and I. Dharssi, 2019: On the soil moisture memory and influence on coupled seasonal forecasts over Australia. *Climate Dyn.*, **52**, 7085–7109, <https://doi.org/10.1007/s00382-018-4566-8>.
- Zhou, J., Z. Zuo, X. Rong, and J. Wen, 2020: Role of May surface temperature over eastern China in East Asian summer monsoon circulation and precipitation. *Int. J. Climatol.*, **40** (4), 1–14, <https://doi.org/10.1002/joc.6588>.
- Zhou, T., L. Zou, and X. Chen, 2019: Commentary on the Coupled Model Intercomparison Project phase 6 (CMIP6). *Climate Change Res.*, **15**, 445–456, <https://doi.org/10.12006/j.issn.1673-1719.2019.193>.
- Zuo, Z., and R. Zhang, 2007: The spring soil moisture and the summer rainfall in eastern China. *Chin. Sci. Bull.*, **52**, 3310–3312, <https://doi.org/10.1007/s11434-007-0442-3>.
- , and —, 2016: Influence of soil moisture in eastern China on the East Asian summer monsoon. *Adv. Atmos. Sci.*, **33**, 151–163, <https://doi.org/10.1007/s00376-015-5024-8>.

Evaluation of Soil Moisture in CMIP6 Simulations

Qiao, Liang; Zuo, Zhiyan; Xiao, Dong

-
- 01 mingxi zhang Page 2
11/9/2024 7:58
- 02 mingxi zhang Page 3
30/10/2024 8:20
- 03 mingxi zhang Page 3
30/10/2024 8:21
- 04 mingxi zhang Page 3
30/10/2024 8:21
- 05 mingxi zhang Page 3
30/10/2024 8:21